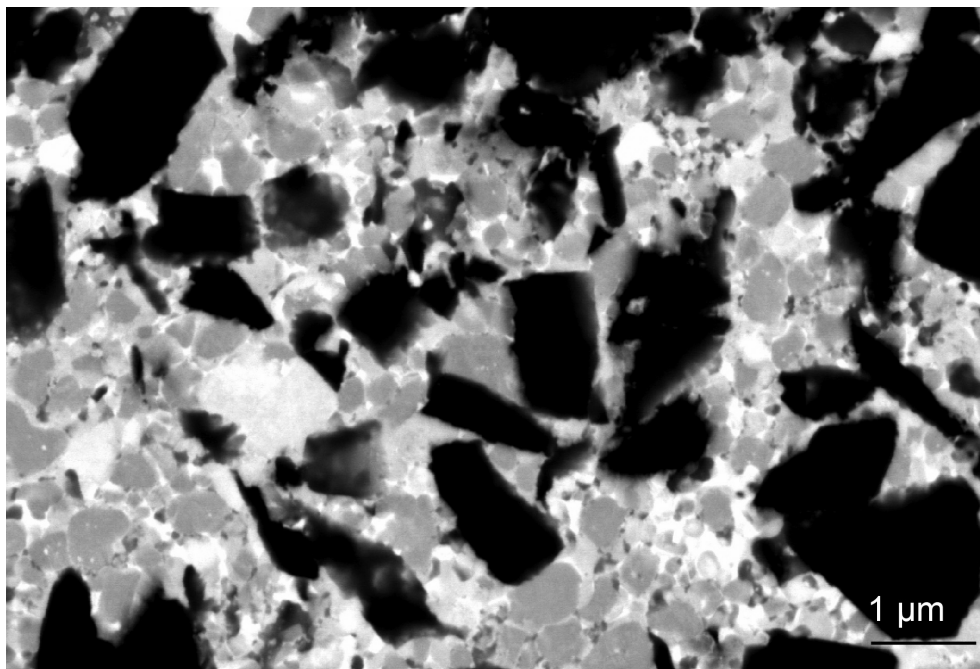# CHALMERS

Characterisation of Polycrystalline Cubic Boron Nitride Tool Materials

Master's Thesis in Applied Physics

KRISTINA LINDGREN

Department of Applied Physics
Division of Materials Microstructure
CHALMERS UNIVERSITY OF TECHNOLOGY
Gothenburg, Sweden 2013

Characterisation of Polycrystalline Cubic Boron Nitride Tool Materials

KRISTINA LINDGREN

Characterisation of Polycrystalline Cubic Boron Nitride Tool Materials

KRISTINA LINDGREN

Department of Applied Physics
Chalmers University of Technology
SE-412 96 Gothenburg
Sweden
Telephone: +46 (0)31 772 10 00

Cover shows a SEM BSE image of a PCBN material fabricated with 2.0 wt% Al, 5.9 wt% W, 5.4 wt% Co, 37.1 wt% Ti, 7.01 wt% C, 24.1 wt% N and 2.65 wt% O. The black grains are cBN.

Characterisation of Polycrystalline Cubic Boron Nitride Tool Materials

KRISTINA LINDGREN
Department of Applied Physics
Chalmers University of Technology

Abstract

The reactions that occur during sintering of polycrystalline cubic boron nitride composite (PCBN) tool materials and their dependence on starting powder composition have been mapped. The starting powder mixtures of the PCBN composites consist of cBN, Ti(C,O,N), Al, and milling body debris. Two different types of milling bodies were used, WC-Co and cermet ((Ti,W)(C,N) grains in a Co binder phase). The PCBN materials were investigated before sintering, after pre sintering ($900\,°\mathrm{C}$) and after high pressure high temperature sintering ($1400\,°\mathrm{C}$) in order to understand the processes taking place. Methods used were XRD and SEM/XEDS. The Al was found to melt during the pre sintering and react with either W or Co. Among the phases found in the high pressure high temperature sintered materials were cBN, Ti(C,O,N), (Ti,W)(C,O,N), AlN, TiB_2, WC, Al_2O_3, W_2CoB_2 and two unidentified phases.

Acknowledgements

During the project many persons have been of great help to me. First of all I would like to thank my supervisors, Lena Falk at Chalmers and Annika Kauppi at Sandvik Coromant. I am very thankful for your help and input.

Then of course, I would like to thank the groups that I have been part of during this spring, the Division of Materials Microstructure at Chalmers, and CTPB at Sandvik Coromant. I am also thankful to the Eva Olsson Group at Chalmers, and the people doing chemical analysis, XRD and the sample preparation at Sandvik Coromant. You have helped me a lot, with both the fabrication and specimen preparation of the materials and learning how to use the instruments. You have also been great company.

Finally, I would like to thank my family and friends. You are all very important to me.

Kristina Lindgren, Gothenburg 18/6 2013

List of Figures

List of Tables

List of Acronyms

APT   Atom Probe Tomography

BET   Brunauer-Emmett-Teller

BSE   Backscattered Electrons

cBN   Cubic Boron Nitride

DI   Diamond Innovations

EELS   Electron Energy Loss Spectroscopy

hBN   Hexagonal Boron Nitride

HPHT   High Pressure High Temperature

PCBN   Polycrystalline Cubic Boron Nitride

PDF   Powder Diffraction File

PEG   Polyethylene Glycol

SE   Secondary Electrons

SEM   Scanning Electron Microscope

TEM   Transmission Electron Microscope

XEDS   X-ray Energy Dispersive Spectrometry

XRD   X-Ray Diffraction

XRF   X-Ray Fluorescence

Contents

1

Introduction

Very hard cutting tools open up for new, improved, ways of forming metals. They might both improve the work environment, the production rate and the performance of the cutting methods. This since very hard materials makes it possible to cut the metal instead of grinding it to its desired shape [1]. Cubic boron nitride (cBN) is the second hardest material known. The properties of cBN makes it possible to use the compound in these kind of cutting tools.

When used in cutting tools the cBN is usually a part of a composite material, in order to make the material sinter. The phases that are created together with the additives affect the properties of the composite and thus it is interesting to investigate and systematise the behaviour of the material depending on composition.

Earlier studies have shown phases present after sintering and their relative positions and amounts. In this project the focus is on characterising and systematising the dependence of the matrix microstructure on the starting powders and milling bodies, and how this affects the sintered material.

Different binder phases might be used for cBN composites. Commonly, variations of TiN, TiC or Ti(C,N) are used [2-4]. In this project Ti(C,O,N) was investigated as matrix phase. Al was added in order to take care of the O from the Ti(C,O,N) and powder particle surface oxides. W and Co from the two different types of milling bodies were present as well. The effect of different amounts of Al, W and Co was investigated in this project.

The project was carried out as a collaboration between Chalmers University of Technology in Göteborg and Sandvik Coromant in Västberga. The fabrication of the materials and X-ray diffraction (XRD) was performed at Sandvik, and scanning electron microscopy (SEM) and X-ray energy dispersive spectrometry (XEDS) was done at Chalmers.

1.1   Aim of the project

The goal of this masters project is to understand what happens to the different phases in a polycrystalline cubic boron nitride composite (PCBN) with different starting powder composi-

tions during the densification process. The amount of Al, Co and W is varied by varying the amount of Al raw material powder, the milling time and the type of milling bodies. In total this gives twelve different compositions. Which phases are created, the amount of each phase and their distribution in the material is investigated in the different manufacturing steps. In each material the processes in the different steps are followed in order to get a better understanding of the reactions taking place. The analysis is done by XRD, SEM and XEDS.

2

Background

This chapter describes some of the background theory needed in order to get an overview of the subject. Firstly, a description of the material and then it continues with a description of sintering, the process used to make the material dense. Also, some of the earlier results in the area are described.

2.1 Cubic boron nitride

Cubic boron nitride (cBN) is the second hardest known material. Only diamond is harder. cBN and diamond basically have the same crystal structure. However, the carbon in the diamond is exchanged for boron and nitrogen in cBN, a sketch of the structure can be seen in Figure 2.1. Unlike diamond, cBN is not present in nature. cBN was synthesised for the first time in 1957 by Wentorf [5]. cBN is manufactured from a hexagonal structure (hBN) at high temperature and high pressure, again a similarity to diamond. A catalyst might lower the required temperature and pressure [6]. The cBN structure is thermodynamically unstable, but the transformation back to hBN is very slow.

2.2 Polycrystalline cubic boron nitride

cBN is very hard and thermally stable at high temperatures [7] which makes it useful for cutting tool applications where a diamond cutting tool would have started to react with the work piece. In most applications a composite of cBN and some more substances are used, called polycrystalline cubic boron nitride (PCBN). This gives the material the wanted properties, for example it might decrease the brittleness of the material.

In this project Ti(C,O,N) was used as a binder phase. Al was added as well in order to react with the oxides on the surfaces of the powder particles of the raw materials and from the Ti(C,O,N). W and Co from the milling process (the milling bodies contain W and Co in different amounts) were also be present in the material.
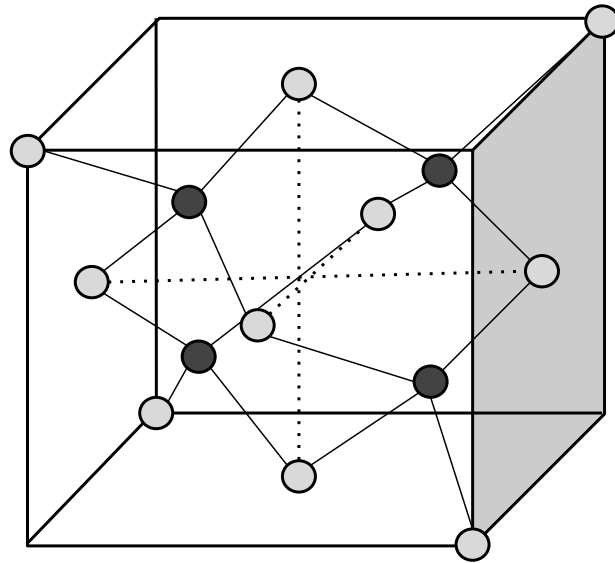
Figure 2.1: The structure of cBN, the same as diamond but with B(bright) and N(dark) instead of only C atoms.

The composite PCBN may contain different amounts of cBN. These have different properties that are interesting for different applications. Low content PCBN contains around 45-60 % cBN, and this type is investigated in this project. These materials are used for finishing and for continuos working of a material. High content cBN has as much as 80-90 % cBN [2] and is used for applications where more material is removed at one time, and when the turning is uneven.

The PCBN material is processed into discs, that are cut into even smaller pieces and soldered into the corners of a hard metal tool. The corners are used for cutting. In this way the expensive cBN is only used where it is needed.

2.3 Fabrication of PCBN materials

In order to fabricate the PCBN composite the raw material powders are generally milled in ethanol. The slurry is then dried. One way of drying the slurry is using a spray drier that blows out the slurry in a warm environment where it forms granules. Polyethylene glycol (PEG) can be added to the slurry before drying in order to form those granules. Granules are wanted since they flow better and thus are easier to handle and pour later in the process. The granules are pressed into green bodies and then pre sintered to get rid of the PEG and form solid discs. These can then be high temperature, high pressure (HPHT) sintered.

2.4 Sintering

The phenomenon sintering is the redistribution of species that leads to pore shrinkage in the green body. This makes the material more dense. The driving force for the changes in the structure is a lowered free energy of the particle surfaces, i e a reduced surface area. A small radius of the particles in a material gives more surface area and thus a high surface energy. Therefore smaller particles generally sinter better than larger ones. A smaller radius also gives a higher curvature and shorter diffusion distances, increasing the sintering speed [8]. There are two different types of sintering; solid phase sintering and liquid phase sintering.

There are three different transport mechanisms in solid state sintering. Evaporation and condensation is one. Another one is surface diffusion where material from the surface of the powder particle move towards the contact point between two powder particles, or the neck where the particles are connected. The matter might come from the particle contact point itself and relocate to build the neck. The third type of transport mechanism for solid state sintering is bulk diffusion. The different transport mechanisms might happen simultaneously, and it might change during the sintering time.

The other type of sintering is liquid phase sintering. In this case the material transport happens with the aid of a liquid phase within the multi component material. Between two particles there is a negative pressure (capillary pressure) compared to the rest of the system, and this results in a flow of matter away from the boundary and forming a neck around it. The process is affected by the viscosity of the liquid (that might be very dependent on the temperature as well), the size of the particles and the surface tension [9]. When the temperature is lowered the liquid phase will become solid again. This type of sintering is in general faster than the solid state sintering.

There are many things happening with the structure of a material when it is sintered. The particles might grow and change size, the number, shape and size of the pores might change, new phases might form, amongst some possible scenarios [9].

The phases created during the sintering might not have reached thermodynamical equilibrium, due to the relatively short time the material is exposed to the temperature and pressure. However this is not necessary an issue. cBN is not a stable phase itself for instance, but very useful since the time scale of transformation back to hBN is very long. The same thing might apply to the phases created during sintering. The sinterability and hence the microstructure is affected by many parameters, like the chemical composition, size and size distribution, stoichiometry, sintering temperature and pressure [10].

2.5 Earlier studies and results

Studies have been done on similar PCBN materials. Angseryd [2] investigated a quite similar material in her doctoral thesis. She studied a PCBN material with a Ti(C,N) matrix, and several different techniques including SEM, XEDS mapping on thin materials, thermodynamical calculations, transmission electron microscopy (TEM), electron energy loss spectroscopy (EELS) and atom probe tomography (APT). She found several phases in her HPHT sintered materials such as $Ti(C_x,N_{1-x})$ with x between 0.5 and 0.7, cBN, TiB_2, Al_2O_3 and AlN. It was also possible

to find WC grains from the cemented carbide milling bodies. The different phases were found in different parts of the microstructure. The TiB_2 was located close to larger Ti(C,N) grains, whereas Al_2O_3 and AlN also had specific locations. APT revealed that the Ti(C,N) phase seemed to act as a diffusion path for other atoms such as B, W, O and Al. However, the cBN grains were mostly preserved during sintering. The phases created were usually in very small volumes, making them hard to investigate due to a high resolution needed. The tool wear was also investigated by Angseryd.

Benko et al. [3, 11] also investigated PCBN composites with different binder phase compositions. cBN-TiN, cBN-TiC and cBN-Ti_3SiC_2 were studied. The materials were fabricated by mixing the powders and sintering them into pellets at high temperature and pressure, thereafter they were heat treated. They performed XRD, TEM and thermodynamical calculations in order to map the phases created. TiB_2 was found in both the TiC and TiN compositions. In the cBN-TiC material also $TiC_{0.8}N_{0.2}$ occurred. In the Ti_3SiC_2 case TiC, TiN, SiC and SiB_4 was formed.

Rong et al [4] also investigated cBN-TiN composites with added Al. They found AlN, TiB_2 and the starting TiN and cBN. They suggested that the reaction

$$2BN + TiN + 3Al \rightarrow 3AlN + TiB_2 \tag{2.1}$$
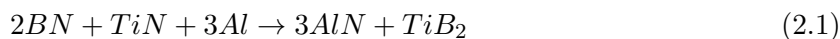
occurred in their materials during densification.

As far as we know today, no studies have been done on PCBN materials with Ti(C,O,N) matrices and not on materials milled with the specific composition of cermet milling bodies. No publications of the characterisation of different compositions were found either.

3

Analytical methods

In this chapter the analytical methods used are explained. Chemical analysis, XRD, SEM and XEDS are all used in the project.

3.1 Chemical analysis

The amount of O, N and C was determined by combustion. The materials were combusted together with some metals and the amount of gas produced was measured. For determination of C contents one measures CO_2, for O and N contents NO_2.

XRF stands for X-ray fluorescence. High energy X-rays are emitted onto the material, and when these excites an inner shell electron, another electron falls down emitting a lower energy X-ray characteristic of the element. This gives information about the elemental composition of the material close to the specimen surface. The analysis depth is dependent on the energy of the incoming X-rays and the chemical composition of the material. A typical depth might be $10\,\mu$m [12].

Specific surface area determination of the milled powder was done in order to see the impact of the milling. This was done by the BET (Brunauer-Emmett-Teller) method. Liquid N is cooled down, then N is condensed on the surfaces of the powder particles. The cooling is removed, which makes the N leave the surfaces of the material. Then the amount of N gas that leaves the material is measured.

3.2 XRD

X-ray diffraction (XRD) is a non-destructive way of getting to know which phases there are in a material. Crystals consists of regular planes of atoms. These will give rise to a diffraction pattern according to Bragg's law. Different crystal structures made out of different atoms give rise to different peak patterns depending on crystal structure and lattice parameters. The intensity as a function of angle is recorded with a detector that rotates around the specimen
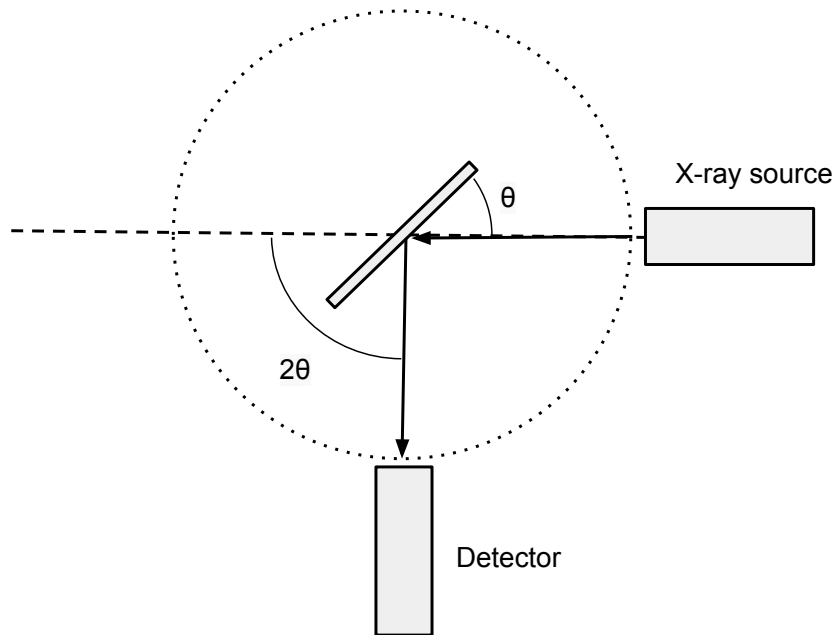
Figure 3.1: The setup of the XRD.

that also rotates in order to maintain the geometry that is shown in Figure 3.1. The angle at which the signal is recorded is 2θ, twice the angle between the specimen surface and the incident X-ray beam.

An identified peak corresponds to an interplanar distance in a certain structure for a set of planes (h, k, l). Then

$$2d_{hkl}\sin\theta = n\lambda \tag{3.1}$$

which is Bragg's law. n indicates which order of spectrum is considered and d_{hkl} is the plane distance. In XRD $n = 1$ is used. For a cubic structure

$$a = d_{hkl}\sqrt{h^2 + k^2 + l^2} \tag{3.2}$$

where a is the lattice parameter and λ is the wavelength [13]. When a Cu anode is used and the Kα line is considered $\lambda =$1.5406 Å. The usage of this information and a data base (PDF - Powder Diffraction File, provided by the International Centre for Diffraction Data) makes it possible to identify the phases. Limitations of the techniques is that very small amounts can not be detected, nor can amorphous materials since they do not have the crystal planes needed for diffraction.

3.3 SEM and XEDS

SEM stands for Scanning Electron Microscopy. Scanning means that the specimen surface is imaged one point at a time, and electron microscopy indicates the usage of electrons instead of
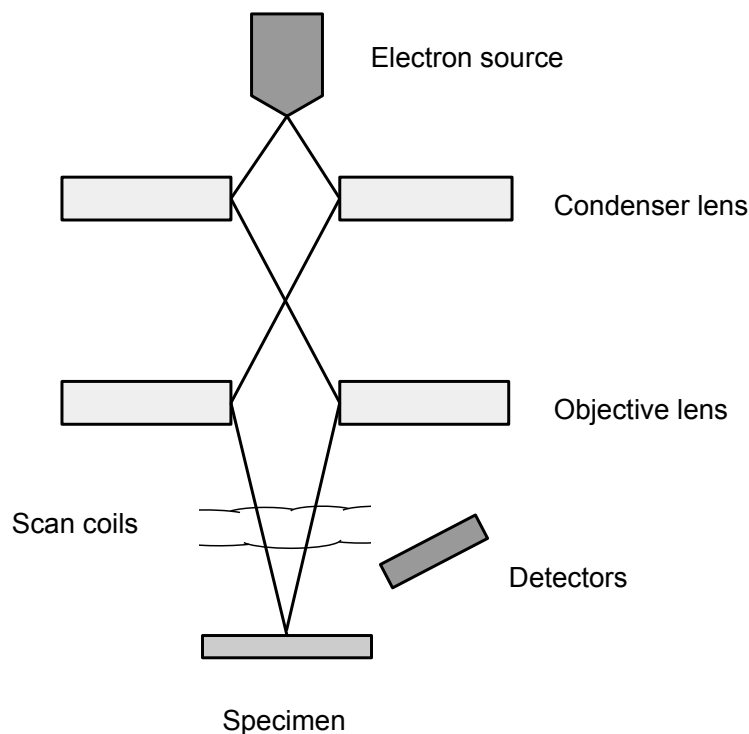
Figure 3.2: The image forming system of an SEM.

electromagnetic radiation such as visible light. The image forming system is sketched in Figure 3.2. The electron source is on top. Condenser and objective lenses focuses the beam, using magnetic fields. The scanning coils steer the beam to scan the specimen surface. The different types of detectors collect the signals.

There are some different modes. Secondary electrons (SE) comes from the volume closest to the surface. Those electrons come from the material itself originally. They give a topographical contrast and have low energy, less than 50 eV, which is a rather arbitrary choice [14]. However, most of those low-energy electrons are really secondary electrons.

The backscattered electrons (BSE) are electrons from the beam of the SEM. BSE give elemental contrast, due to the higher cross section for electron scattering for heavier atoms. The heavier atoms, the more backscattered electrons and the brighter the image contrast. The escape depth is slightly larger than that of the SE and the higher energy makes it possible to detect them separately from the SE.

However, it is possible not only to image but also to perform chemical analysis in the SEM. A third type of signal detected the SEM is X-rays generated in the material by the electron beam. The analysis of these is called XEDS, X-ray energy dispersive spectrometry. The beam electrons excite the inner shell electrons of the atoms in the material and these leave room for other electrons to fill. When the electron falls down, energy is emitted as an X-ray photon. The energies of such transitions are characteristic of every element. In this way chemical information
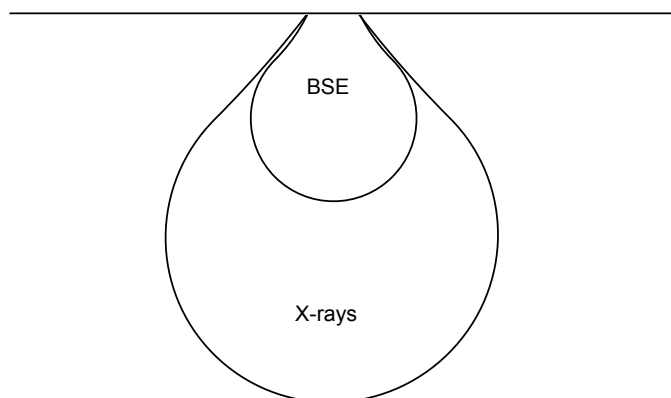
Figure 3.3: The X-rays come from a larger volume than the backscattered electrons (BSE).

of the composition of the material is achieved. However, it is harder to quantify the elements than to qualify them. The ratio of the measured intensity of the peaks is not simply the ratio of the concentrations of the elements. Especially lighter elements are problematic. There is also a continuous background called Bremsstrahlung ("brake radiation") coming from the interaction of the electrons from the beam and the coulomb field of the atom nucleus. The volume from which the detected X-rays come is even larger than the one for BSE, giving a lower spacial resolution.

When using SEM an important factor for the resolution is the volume from where the signal comes. As described above the different modes of operation have different sizes of this volume, as can be seen in Figure 3.3. This affects the resolution of imaging and analysis. The volume is strongly dependent on the accelerating voltage. Electrons with higher energies penetrate deeper into the material. The cross section for elastic scattering is proportional to $1/E^2$, the inverse of the squared energy [14]. Therefore, a lower voltage gives higher resolution. However, a lower voltage gives a weaker signal. For XEDS, the accelerating voltage needs to be higher than the energy needed to knock out the electron, which makes the accelerating voltage a trade off factor. The cross section for elastic scattering is proportional to the atomic number squared, Z^2, giving different interaction volumes for different elements [14].

4

Experimental procedures

Here the practical part of the experiments are presented, as well as the instrumentation. An overview of what was done can be seen in Figure 4.1. The raw material powders were mixed, milled and dried in the powder process. Then the granules were formed into green bodies, pre sintered and finally sintered in high pressure and high temperature (HPHT). XRD was carried out in all three steps. After the powder process chemical analysis was performed, and after the two sintering steps SEM was used in order to investigate the microstructure.

Figure 4.1: Overview of the process.

4.1 The powder process

The process of making the materials has several steps. First, the Ti(C,O,N) powder (out of the C,O and N, 71 % was C, 6 % N and 23 % was O; from Treibacher) was pre milled. This was done in an attritor mill with ethanol (and nitrogen gas) in order to reduce the size of the powder particles. After this Al and cBN were added to the slurry, and it was milled again. The reaso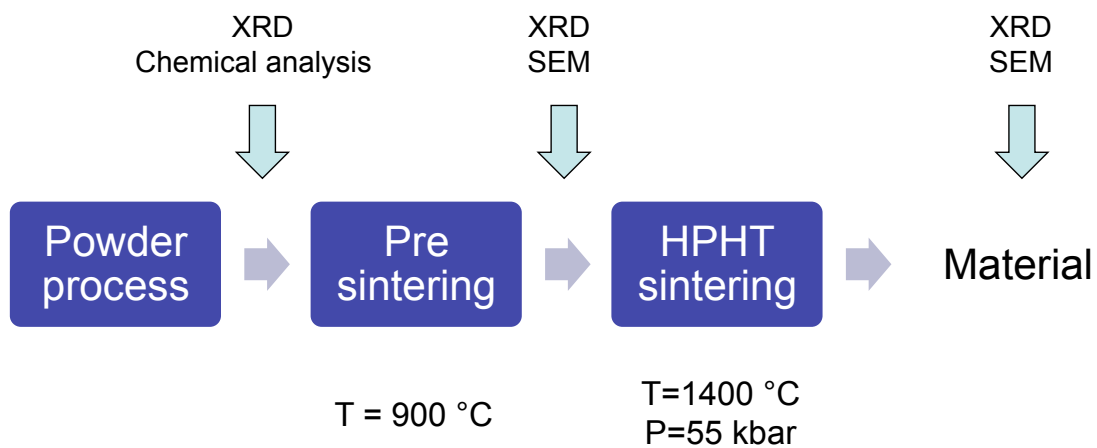n for pre milling the Ti(C,O,N) is that it seems to get stuck between the hard cBN particles otherwise, and not getting milled. The cBN is very hard, making debris from the milling bodies join the slurry. Both the pre milling time and the milling time was different for the different batches, since this is the way to vary the amount of W.

After the milling some PEG (polyethylene glycol) was added, in order to bind the granules together in the spray drying process. This in turn, makes the granules flow easier. A good flow makes the handling of the granules easier since the shaping form does not have to be hand filled.

The slurry was spray dried in order to form granules that can later be sintered. The spray dryer used was a table top Büchi. The size of the granules are dependent on various factors including the viscosity of the slurry and the temperature and air flow of the spray dryer.

4.2 Powder characterisation

Chemical analysis was performed in order to determine the chemical composition of the milled starting powder mixtures. The analyses were performed by the chemical analysis group, and by their standard methods, at Sandvik Coromant in Västberga.

For XRF the not yet spray dried powders are oxidised at high temperature, then mixed with lithium borate and melted into a glass in the shape of a small puck. The addition of lithium borate made it impossible to measure boron with this technique. The XRF was performed on these pucks. The amounts of C, O and N were not possible to measure with XRF, since those elements are combusted in the material preparation process.

The spray dried granules were investigated with XRD. They were packed into the specimen holder of the instrument by hand.

4.3 Sintering

After spray drying, the granules were sent to Diamond Innovations (DI), for pre sintering and HPHT sintering. At DI the granules were pressed into green bodies that were around 50 % dense. In the pre sintering the temperature was increased quite fast, but at 200 °C the rate was decreased so that the materials would not break due to the gas that was created when the PEG was leaving the compact. During heating up to 400 °C a hydrogen atmosphere was used to make the PEG leave easier. After this the process was carried out in vacuum and the temperature was increased slightly faster. The compact was held at 900 °C for 15 minutes.

Thereafter it was time for the HPHT sintering process. This was done in a large cell. Four of the pre sintered PCBN discs were stacked with cermet discs and layers of mica, graphite and Mo. The graphite was used since it is a good heat conductor. However, the graphite may react with the cermet discs and PCBN discs. Mo film was used closest to the cBN, since these films

are flat and quite inert. Mica layers were present close to the cermet disc. The HPHT process took place in several steps. First, the pressure was increased, then the temperature, and then both of them. The materials were held at 1400 °C and 55 kbar for 45 minutes.

4.4 Specimen preparation

After the HPHT sintering small (13 mm in diameter) discs and squares (5 mm) were cut from the larger discs (around 6 cm). Specimens were taken from both the centre and the edge of the sintered discs. This was done at DI as well. The small discs or squares were then polished, to remove the Mo films still there on some of the discs, and to get a flat surface for the SEM and XRD investigations. In order to do this they were first moulded into Bakelite and then polished in several steps. In the last step a diamond slurry of $1\,\mu$m was used. After polishing the Bakelite was removed in order to fit the materials into the specimen holders in the SEM and the XRD. For SEM the specimens were carefully cleaned in ultrasonic cleaner in acetone and ethanol and then attached to aluminium specimen holders by carbon tape or silver paint.

The pre sintered materials was crushed in a mortar and powder diffraction was performed, just as before sintering. The pre sintered materials were investigated in SEM as well. Their porous structure made it hard to get a cut through the grains for SEM imaging of a cross section. Instead, the pre sintered material was broken and the powder like structure of the fracture surface was imaged. This made it possible to study the outside of the grains.

4.5 Instrumentation

Chemical analysis by combustion was carried out in a LECO TC436DR for the determination of O and N content. LECO CS444 was used for C content determination. A PANanalytical Omnian instrument was used for XRF. The specific surface area determination of the milled powder was done in a Monosorb instrument. The XRD was done on a PANalytical X'pert Pro operating at 45 keV and 40 mA using a Cu Kα X-ray source. A PANalytical Cubix[3] with Cu Kα X-ray source operated at the same voltage and current was also used for the XRD measurements. All those instruments are placed at Sandvik in Västberga.

Two different SEMs were used, Fei Quanta 200 FEG ESEM and Leo Ultra 55 FEG SEM. The environmental mode in the ESEM was not used, everything was done in high vacuum. Mainly the BSE mode was used. The accelerating voltage in the ESEM was 10 keV, spot size 3 and working distance 6 mm to 10 mm. The ESEM was mainly used for overview micrographs due to its lower resolution. The accelerating voltage for the Ultra SEM was set to 8 keV to 12 keV, aperture $60\,\mu$m, working distance 4 mm to 10 mm. XEDS analysis was performed in the Ultra. For XEDS the working distance was 8 mm and the accelerating voltage was 8 kV. The XEDS system was an INCA from Oxford instruments.

5

The materials - test plan

In this project twelve different materials were studied. In all materials the amount of cBN was around 50 wt%. The test plans for those are shown in Tables 5.1 and 5.2. Two different types of milling bodies were used, WC-Co and cermet. The chemical compositions of these are shown in Table 5.3. The amounts of both W and Co are dependent on the type of milling bodies used, since they will add different amounts of their own composition during the milling process. The very different milling times for the two types of milling bodies is because of the large difference in the W content of the two types of milling bodies.

The amount of W was varied in three steps; 3 wt%, 6 wt% and 9 wt%, by using different milling times. The amount of Al was also varied, one lower and one higher amount were tested. The lowest amount of Al was decided in order react with all the O in the material to form Al_2O_3. In the test plan tables, 1 means that approximately all the Al would form Al_2O_3, and 2 means that twice as much Al was added.

5.1   The milling bodies

The two types of milling bodies were very different. WC-Co is commonly used in milling bodies. The WC-Co is a structure consisting of grains of hexagonal WC in a face centred cubic Co binder phase. The amount of W is much larger than the amount of Co, as can be seen in Table 5.3.

In this project, cermet milling bodies consisting of (Ti,W)(C,N) grains in a Co binder phase were used as well. By cermet (from the words ceramic and metal) one usually means a Ti(C,N) structure, without WC, used for cutting tool materials [15]. The reason for trying this type of milling body is to increase the milling time and hence possibly get a better distribution of the constituents in the material. The grains consisting of (Ti,W)(C,N) are chosen since it is basically the same as the Ti(C,O,N) of the raw material used. The (Ti,W)(C,N) structure, however, have a core-rim structure, with grain centres from the original raw material powder and rims with varying amount of W that are formed during sintering. The binder phase consists of the elements that was liquid during sintering, in this case mainly Co, also in a face centred

cubic structure. Elements from the hard phase (Ti,W)(C,N) are soluble in the binder phase [15]. In total, this makes the cermet structure a quite inhomogeneous one, with very varying amounts of W in different parts of the structure.

Table 5.1: Test plan for batches 1-6. Al/O indicated the amount of Al. During pre milling only Ti(C,O,N) is milled, and for the milling the cBN and Al is added as well.

Material	wt.% W	Milling body	Al/O	Pre milling time	Milling time
1	3	WC-Co	1	30 min	15 min
2	6	WC-Co	1	30 min	37 min
3	9	WC-Co	1	30 min	60 min
4	3	WC-Co	2	30 min	15 min
5	6	WC-Co	2	30 min	37 min
6	9	WC-Co	2	30 min	60 min

Table 5.2: Test plan for batches 7-12. Al/O indicated the amount of Al. During pre milling only Ti(C,O,N) is milled, and for the milling the cBN and Al is added as well. * indicates that this batch was milled at 200 rpm instead of 300 rpm, hence the longer milling time.

Material	wt.% W	Milling body	Al/O	Pre milling time	Milling time
7	3	Cermet	1	12 h*	5 h*
8	6	Cermet	1	8 h	6 h 25 min
9	9	Cermet	1	8 h	10 h 20 min
10	3	Cermet	2	8 h	2 h 40 min
11	6	Cermet	2	8 h	6 h 25 min
12	9	Cermet	2	8 h	10 h 20 min

Table 5.3: The chemical compositions of the milling bodies, from chemical analysis.

Milling body	W (wt%)	Co (wt%)	C (wt%)	Ti (wt%)	N (wt%)
WC-Co	88.0	5.96	5.73		
Cermet	17.8	17.0	9.31	49.0	4.75

6

Results

This chapter presents the results, first the results of the WC-Co milled materials are presented, and then the results for the cermet milled materials. Chemical analysis, XRD spectra, SEM micrographs and XEDS data are included.

6.1 WC-Co milled materials

The results for the more conventional WC-Co milled materials are given first.

6.1.1 Chemical analysis

The chemical compositions of the starting powder mixtures evaluated in the chemical analysis described above are shown in Table 6.1. The amount of W is slightly higher than the test plan. The results from the determination of the specific powder surface area are displayed in Table 6.2. An increase in milling time makes the area larger.

Table 6.1: Chemical composition of starting WC-Co milled powder mixtures in weight percentages from the chemical analysis. The amount of B is not measured in those analyses.

Material	Al (wt%)	W (wt%)	Co (wt%)	Ti (wt%)	C (wt%)	N (wt%)	O (wt%)
1	3.2	3.2	0.2	40.6	7.75	25.9	3.14
2	3.0	6.5	0.5	39.2	7.69	24.8	2.98
3	2.9	10.4	0.8	36.5	7.42	24.4	2.93
4	6.1	3.2	0.3	37.0	7.16	26.5	2.91
5	5.6	6.5	0.6	36.3	7.13	25.7	2.89
6	5.5	10.3	0.7	33.3	6.82	25.6	2.76

Table 6.2: The specific powder surface area of the WC-Co milled powders together with the milling times.

Material	Specific area (m^2/g)	Pre milling time	Milling time
1	3.80	30 min	15 min
2	3.87	30 min	37 min
3	4.14	30 min	60 min
4	3.65	30 min	15 min
5	4.06	30 min	37 min
6	4.21	30 min	60 min

6.1.2   XRD spectra

For each material, there is one spectrum before sintering, one after pre sintering and one after HPHT sintering. The 2θ intervals of the figures are chosen such that the most interesting peaks are visible, and thus the ranges of the different spectra are different. The spectra containing cBN have been shifted in 2θ so that the cBN peaks overlap. The lattice parameter of cBN is not expected to change during sintering. The spectra in a figure are adjusted in height so that more than one spectrum is visible. This makes it easy to compare spectra.

The spectra of the starting powders and the pre sintered and HPHT sintered materials are shown in Figures 6.1, 6.2 and 6.3. The vertical coloured lines are markers for different phases from the powder diffraction data base [16]. The three materials with the lowest Al content are the ones at the bottom in the spectra, and the high Al ones are on top. The milling time is increased from bottom to top for both low Al content and high Al content materials. This means that material 1 is the one closest to the 2θ-axis and then material 2, 3, 4, 5 and 6 are above. The light green spectrum at the top is the Ti(C,O,N) starting powder, used as a reference since this specific stoichiometry of Ti(C,O,N) was not available in the data base. This spectrum is not adjusted in 2θ since there is no known phase to adjust to in the spectrum.

In Figure 6.1 the spectra of the materials before sintering are displayed. In these cBN, Ti(C,O,N), Al, and WC from the milling bodies are identified. The cBN and Ti(C,O,N) peaks all have approximately the same intensity for the different materials. However, the Al peaks are higher for the high Al content materials, and the intensity of the WC peaks gets higher the longer milling time. The positions of the peaks seem to be fairly the same for all materials. All the peaks visible are from the added raw materials. The milling body binder phase (Co) is not visible, probably since the amount is very small. Amounts under approximately 5 vol% are usually not possible to detect with XRD. The WC peaks have quite low height, and the Co is only 6 wt% of the milling bodies.

During the pre sintering, the Al starts to react. In Figure 6.2 the Al peaks are gone, and instead Al_4W and Al_5W have appeared. The WC peaks have disappeared as well in some of the materials.

After HPHT sintering the materials have transformed further as seen in Figure 6.3, implying even more reactions. Except from the cBN and Ti(C,O,N) peaks there is still some WC and
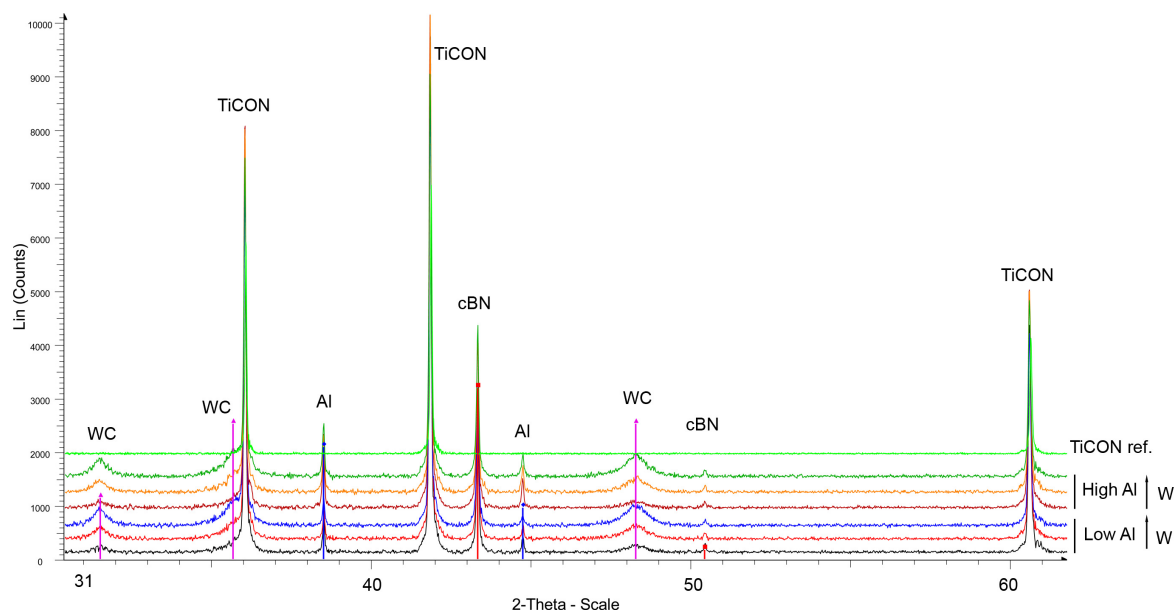
Figure 6.1: XRD spectra for materials 1-6 powder mixtures and the raw material Ti(C,O,N).

now also TiB_2, AlN, Al_2O_3 and W_2CoB_2, but not all in all materials. WC is still present in the low Al, medium and long milling time materials, but seem to have disappeared from the high Al, high W material (material 6) where it was present before. Al_2O_3 seems to be present in all materials, but AlN only in the high Al content ones. W_2CoB_2 is mostly present in the two materials with long milling time. The W_2CoB_2 peaks have a small offset, as can be seen by comparing the spectra peaks with the orange markers in the figure. This might be due to slightly different stoichiometry maybe a slightly different composition of W, Co and B or some other elements present in the structure as well.

The phases found in the XRD spectra after pre sintering and HPHT sintering are presented in Tables 6.3 and 6.4. After pre sintering all spectra contain cBN and Ti(C,O,N). All except for material 4 contain Al_4W. Material 4 does instead contain Al_5W. Materials 2, 3 and 6 contain WC. After HPHT sintering all materials contain cBN, Ti(C,O,N), TiB_2 and Al_2O_3. WC is now only present in materials 2 and 3. AlN is present in materials 4, 5 and 6 and W_2CoB_2 in materials 2, 3 and 6.

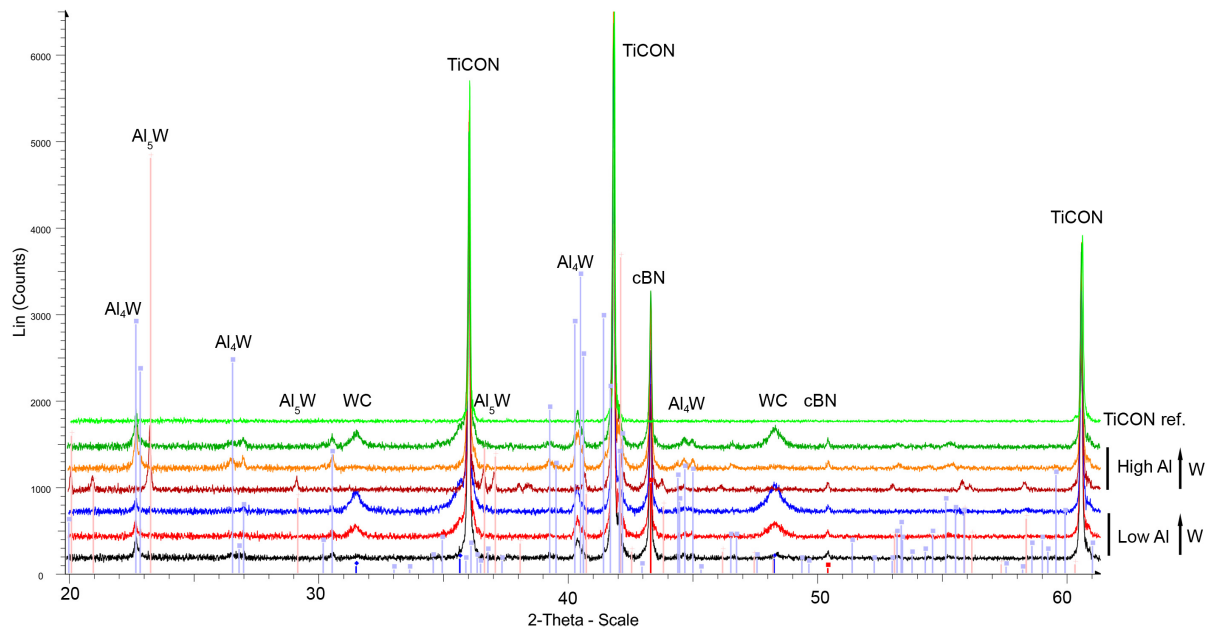**Figure 6.2:** XRD spectra for materials 1-6 after pre sintering and the raw material Ti(C,O,N). Al_4W is marked with light blue lines and Al_5W is marked with pink lines.
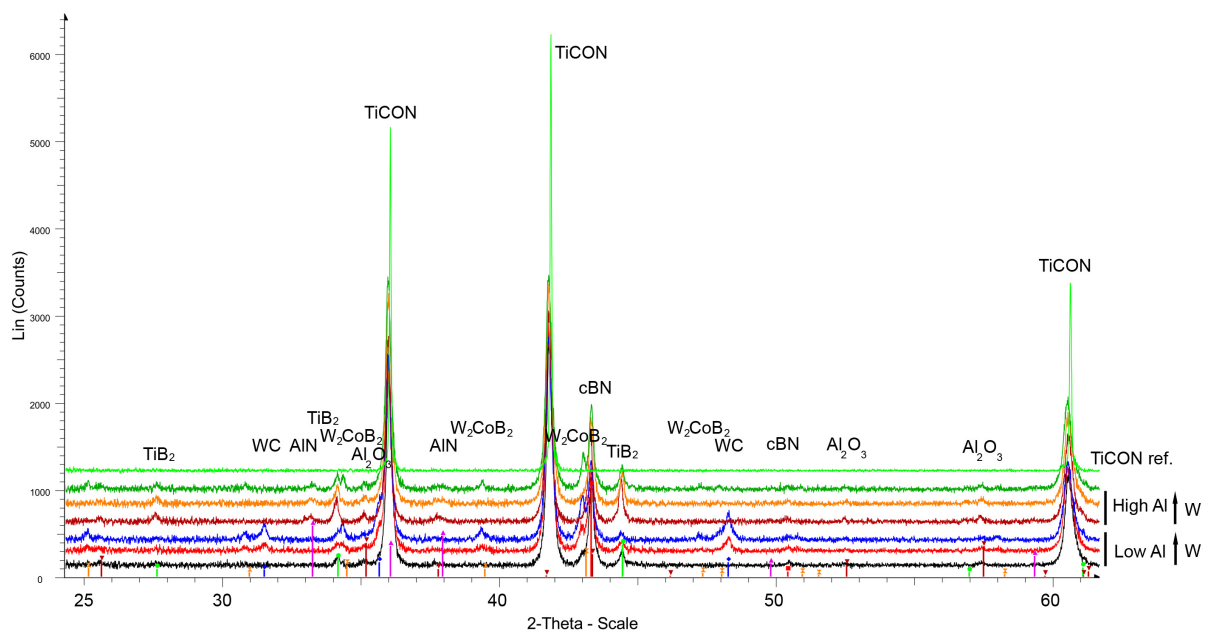

Figure 6.3: XRD spectra for materials 1-6 after HPHT sintering and the raw material Ti(C,O,N).

Table 6.3: The amount of Al, Co and W from chemical analysis and the phases present in the XRD spectra after pre sintering for materials 1-6.

Material	Al (wt%)	W (wt%)	Co (wt%)	Phases
1	3.2	3.2	0.2	cBN, Ti(C,O,N), Al_4W
2	3.0	6.5	0.5	cBN, Ti(C,O,N), Al_4W, WC
3	2.9	10.4	0.8	cBN, Ti(C,O,N), Al_4W, WC
4	6.1	3.2	0.3	cBN, Ti(C,O,N), Al_5W
5	5.6	6.5	0.6	cBN, Ti(C,O,N), Al_4W
6	5.5	10.3	0.7	cBN, Ti(C,O,N), Al_4W, WC

Table 6.4: The amount of Al, Co and W from chemical analysis and the phases present in the XRD spectra after HPHT sintering for materials 1-6. Major phases are the ones with higher intensity in the XRD spectra, and minor phases have lower intensity peaks but still more than one peak to make the identification probable.

Material	Al (wt%)	W (wt%)	Co (wt%)	Major phases	Minor phases
1	3.2	3.2	0.2	cBN, Ti(C,O,N), TiB_2	Al_2O_3
2	3.0	6.5	0.5	cBN, Ti(C,O,N), TiB_2, WC	Al_2O_3, W_2CoB_2
3	2.9	10.4	0.8	cBN, Ti(C,O,N), TiB_2, WC	Al_2O_3, W_2CoB_2
4	6.1	3.2	0.3	cBN, Ti(C,O,N), TiB_2	Al_2O_3, AlN
5	5.6	6.5	0.6	cBN, Ti(C,O,N), TiB_2	Al_2O_3, AlN
6	5.5	10.3	0.7	cBN, Ti(C,O,N), TiB_2	Al_2O_3, AlN, W_2CoB_2

Ti(C,O,N) lattice parameters

A magnification of the 200 peak from Ti(C,O,N) in all spectra of material 6 (5.5 wt% Al, 10.3 wt% W, 0.7 wt% Co) is shown in Figure 6.4. The peak changes position during the HPHT sintering. Table 6.5 contains the calculated lattice parameters for the Ti(C,O,N) during the different steps in the sintering process using equation 3.2 and assigning each peak to a set of hkl that is allowed in the Ti(C,O,N) structure. Ti(C,O,N) has a NaCl structure and the allowed reflections are from planes with hkl 111, 200, 220, 311 and so on.
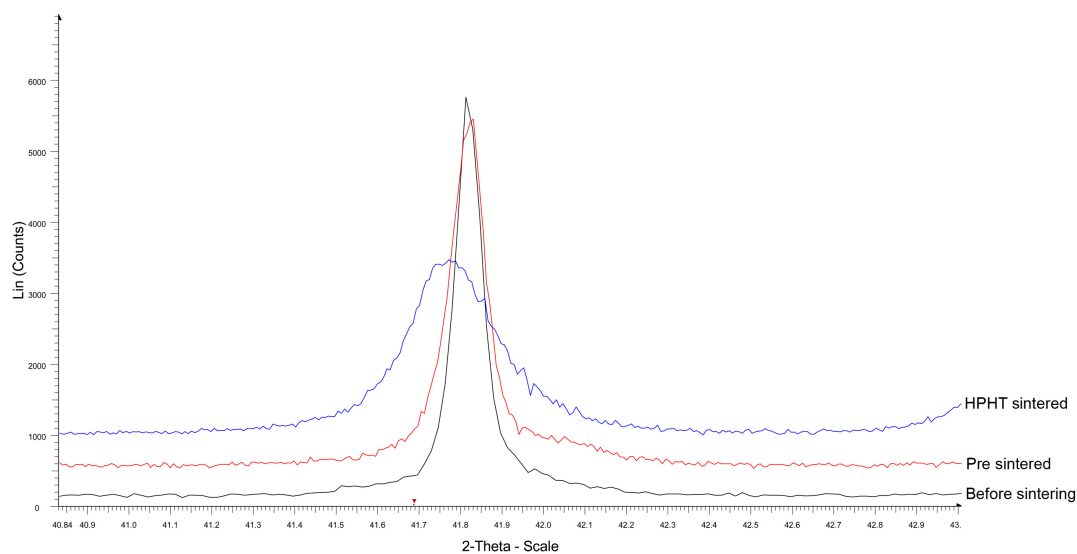
Figure 6.4: The Ti(C,O,N) 200 peak for material 6 (5.5 wt% Al, 10.3 wt% W, 0.7 wt% Co). The black spectrum is before sintering, the red the pre sintered and the blue the HPHT sintered material.

Table 6.5: Lattice parameter of Ti(C,O,N) during the process for the WC-Co milled materials.

Material	a before (Å)	a pre sint. (Å)	a HPHT sint. (Å)
1	4.316	4.317	4.319
2	4.316	4.317	4.321
3	4.317	4.317	4.321
4	4.317	4.317	4.320
5	4.317	4.317	4.320
6	4.317	4.317	4.322

Figure 6.5: The pre sintered material 4 (6.1 wt% Al, 3.2 wt% W, 0.3 wt% Co).

6.1.3 SEM and XEDS of the pre sintered materials

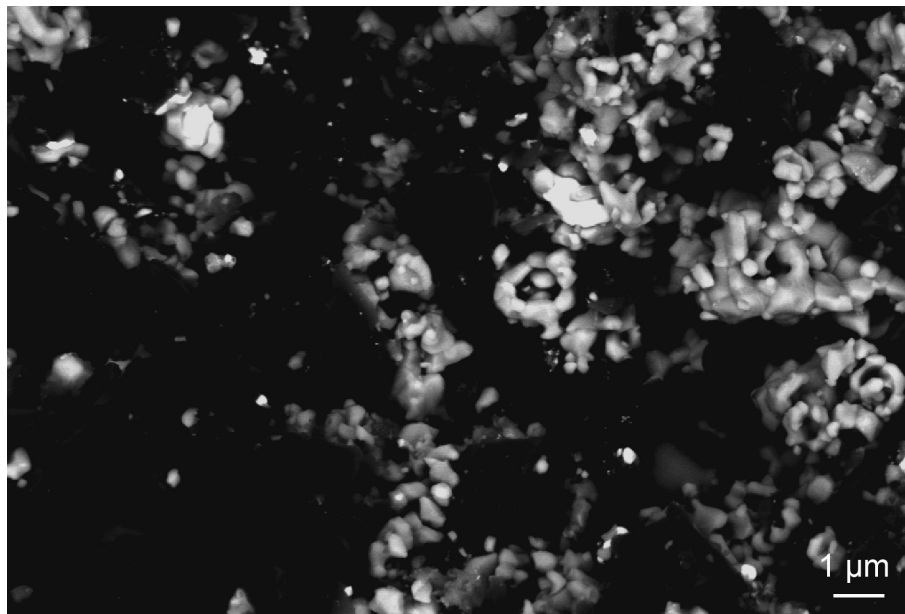SEM and XEDS were performed on the pre sintered and HPHT sintered materials. The main part of this work is done on the HPHT sintered materials.

Two of the pre sintered materials were chosen for SEM and XEDS. The XRD spectra were used for this, picking the one containing Al_5W (material 4 (6.1 wt% Al, 3.2 wt% W, 0.3 wt% Co)) and one containing Al_4W and some WC (material 6 (5.5 wt% Al, 10.3 wt% W, 0.7 wt% Co)). Overviews of the two microstructures taken with the backscatter detector are shown in Figures 6.5 and 6.6. The pre sintered parts were broken into small pieces and the areas studied were on the fracture surfaces. This means that it is not a true cross section of the material that is observed.

When looking at the images of the pre sintered materials it is important to remember that the structures are still very porous (about 50 %). Thus, the black areas in the images might both correspond to holes in the structure and to the lightest phase present in the material, in this case cBN.

Further close ups are shown in Figures 6.7 and 6.8. The arrow in Figure 6.7(a) marks a structure that looks like it has sintered. XEDS was used in order to identify the different phases. However, only the cation % is given here since there are uncertainties in the quantification of the lighter elements. Notice the difference between cation % and wt %. The XEDS spectra also contained one or more of the C, O, B or N peaks (but those are in most cases not mentioned below). The numbers given by XEDS are not exact. The beam spreading and the depth of signal (described in Figure 3.3) are important to remember when interpreting the results, especially when very small features are studied. The signal might come from features hidden under the
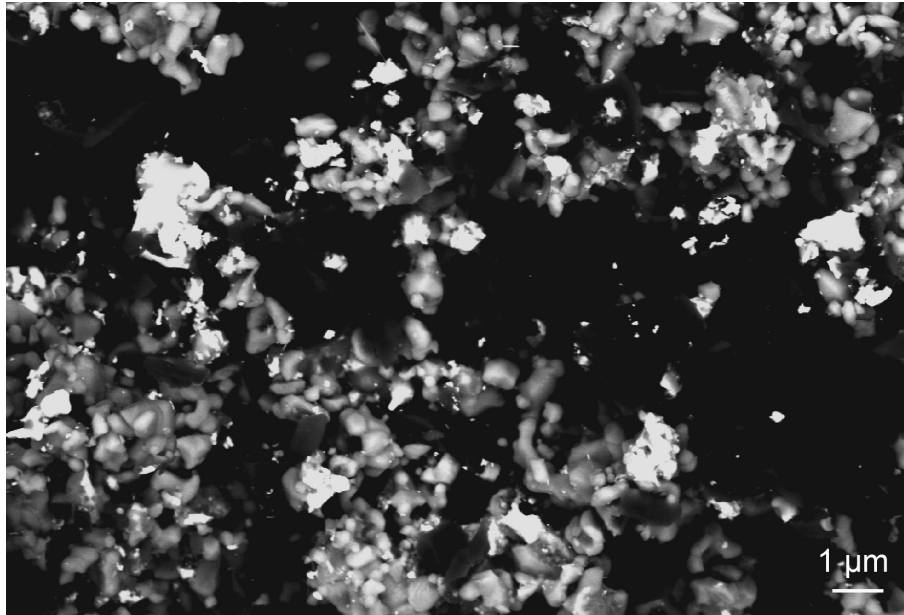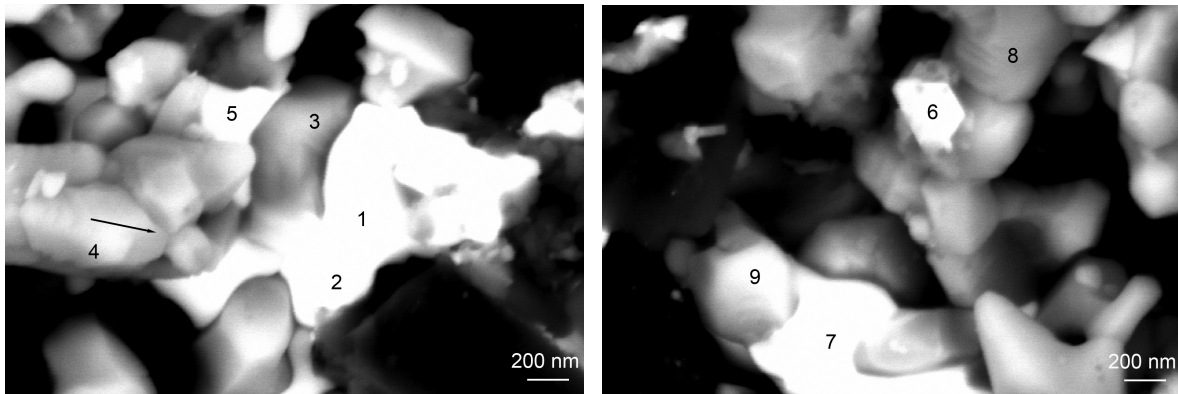
Figure 6.6: The pre sintered material 6 (5.5 wt% Al, 10.3 wt% W, 0.7 wt% Co).

surface, or slightly between the investigated areas.

The lighter areas correspond to phases with higher atomic number. W is the heaviest element in the material with the atomic number 74, and should give a bright contrast to the phases containing it (from XRD Al_4W, Al_5W and WC are known).

(a) The pre sintered material 4 (6.1 wt% Al, 3.2 wt% W, 0.3 wt% Co) at higher magnification

(b) The pre sintered material 4 (6.1 wt% Al, 3.2 wt% W, 0.3 wt% Co) a bit further away

Figure 6.7: The pre sintered material 4 (6.1 wt% Al, 3.2 wt% W, 0.3 wt% Co). The XEDS results for the marked areas are presented in Table 6.6.

Table 6.6: The XEDS results for the areas marked in Figure 6.7. Co was not found in these areas.

Area	W (cat%)	Al (cat%)	Ti (cat%)
1	9.7	90.3	0.0
2	9.5	90.5	0.0
3	4.1	37.2	58.7
4	0.0	9.5	90.5
5	8.8	86.3	4.8
6	10.9	73.5	15.6
7	10.1	89.9	0.0
8	0.0	85.0	15.0
9	0.0	21.5	78.5
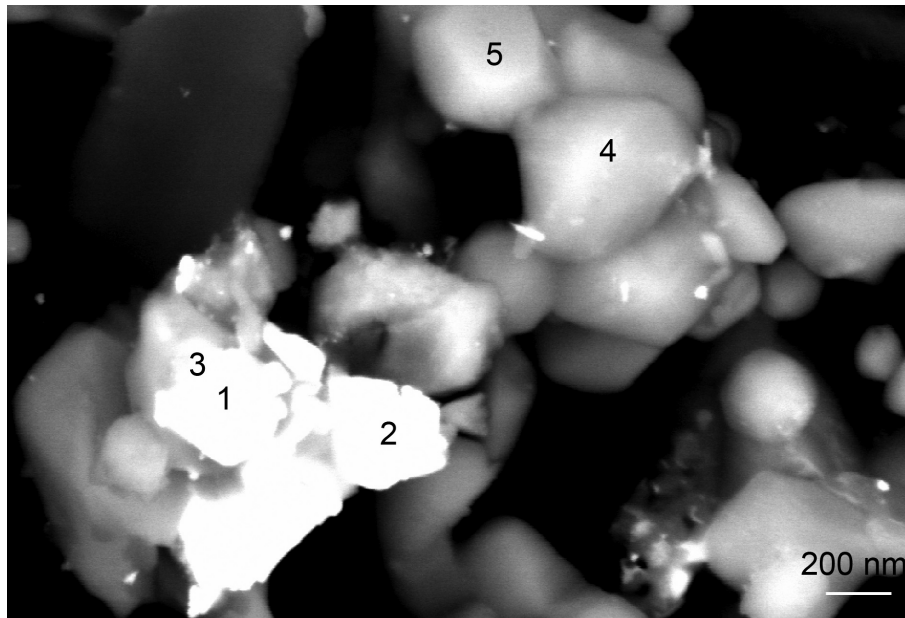
Figure 6.8:   The pre sintered material 6 (5.5 wt% Al, 10.3 wt% W, 0.7 wt% Co) at higher magnification. The XEDS for the marked areas are presented in Table 6.7.

Table 6.7: The XEDS results for the different areas marked in Figure 6.8.

Area	W (cat%)	Al (cat%)	Ti (cat%)	Co (cat%)
1	75.4	24.6	0.0	0.0
2	80.8	19.2	0.0	0.0
3	53.3	37.3	0.0	9.4
4	0.0	7.8	92.2	0.0
5	0.0	8.6	91.4	0.0

6.1.4 SEM and XEDS of the HPHT sintered materials

After HPHT sintering the SEM images look completely different. Now, the materials are dense and the specimen surface have been polished. The imaged surfaces are now cross sections of the materials. An overview of materials 1 to 6 is shown in Figure 6.9. A first glance at these structures gives a lot of information. The black areas correspond to the phase containing the lightest elements and should thus be cBN. The edges of the cBN grains do still look quite sharp. The phases with white contrast do probably contain W. These phases seem to be concentrated to certain areas, probably areas where the WC grains were located before sintering. A W containing phase has formed a network around the grains with light grey contrast. The light grey grains are rich in Ti. There are also smaller particle like features of darker grey contrast between the light grey grains. Those generally contain Al. In material 1 and 4 these seem to be larger and more circular. The different features are marked in Figure 6.9(a). In order to identify the different phases higher magnifications were used.

Close-up

A close up of material 1 (3.2 wt% Al, 3.2 wt% W, 0.2 wt% Co) is shown in Figure 6.10. The XEDS results from the different areas marked in the figure are shown in Table 6.8. The compositions of the different areas in Figure 6.10 varies. No Co was found. The XEDS gave signal for both Al and Ti in all marked areas, but only in two for W.

Figure 6.10 is fairly descriptive for some of the most common structures in the HPHT sintered materials. The dark grey phases containing a lot of Al, area 1, 2 and 3, are probably Al_2O_3 or AlN. However, it is not possible to say which one, since both O and N are very light elements and thus XEDS is not giving reliable results for those (in fact, it did not find neither of the elements in this case, but some O in similar places). The XRD spectrum (Figure 6.3) makes it more possible that it is Al_2O_3, since the AlN peak for material 1 is barely detectable. The high amount of Ti in area 2 and 3 might indicate that the Al-rich phase is very thin and thus a lot of signal comes from the surrounding Ti-rich phase. Area 4 and 5 are the only areas containing some W and also have the brightest contrast. Exactly which phase the W is in is impossible to say from those investigations since so much of the signal comes from the surroundings of the areas of interest. Area 6 and 7 contain mostly Ti, but also some Al cations (15.5 cat% and 10 cat% respectively).
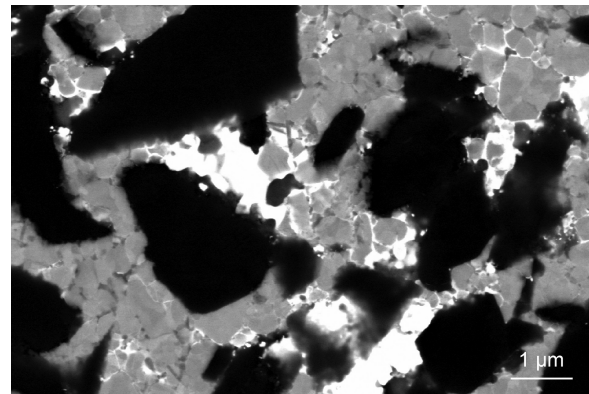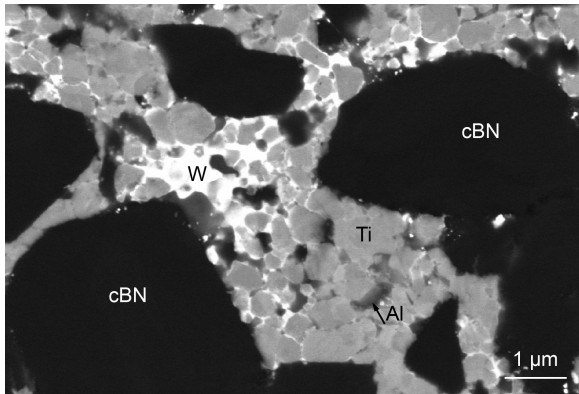
(a) Material 1 (3.2 wt% Al, 3.2 wt% W, 0.2 wt% Co). (b) Material 2 (3.0 wt% Al, 6.5 wt% W, 0.5 wt% Co).
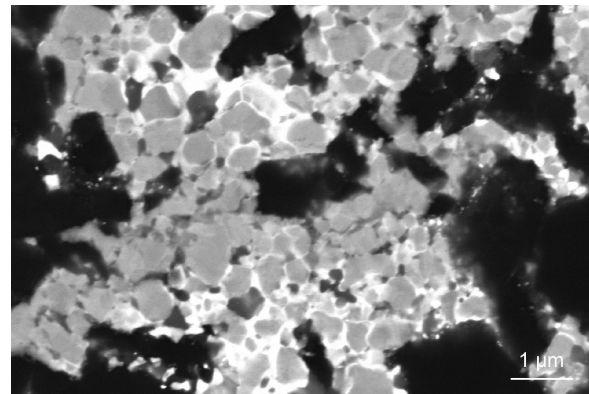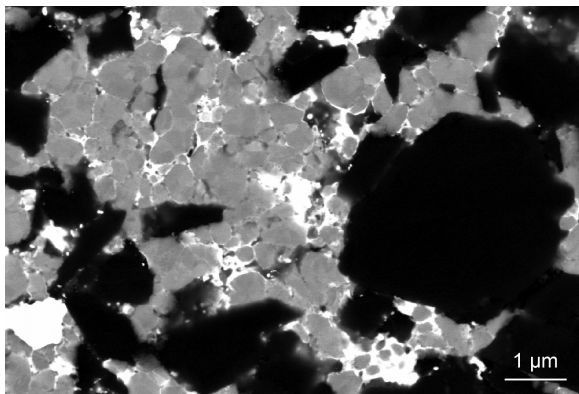
(c) Material 3 (2.9 wt% Al, 10.4 wt% W, 0.8 wt% Co). (d) Material 4 (6.1 wt% Al, 3.2 wt% W, 0.3 wt% Co).
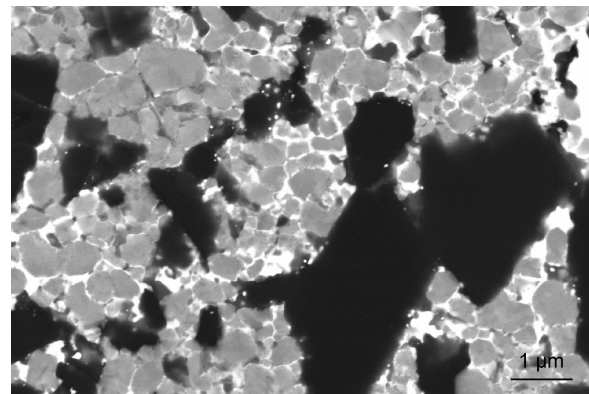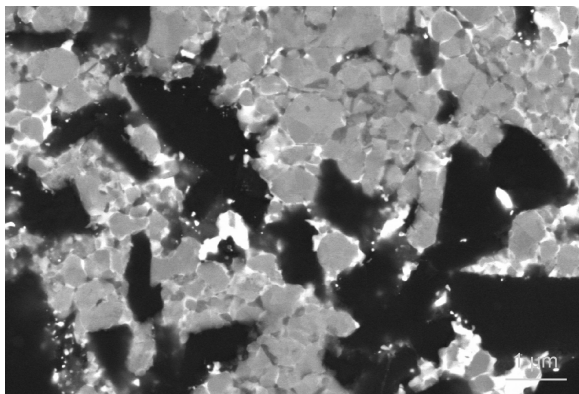
(e) Material 5 (5.6 wt% Al, 6.5 wt% W, 0.6 wt% Co). (f) Material 6 (5.5 wt% Al, 10.3 wt% W, 0.7 wt% Co).

Figure 6.9: Overview of all the HPHT sintered WC-Co milled materials. Areas with black contrast are cBN, grey is rich in Ti, dark grey is Al-rich and white is W-rich phases. In (a) these different phases are marked.

Figure 6.10: The HPHT sintered material 1 (3.2 wt% Al, 3.2 wt% W, 0.2 wt% Co). XEDS for the marked areas are found in Table 6.8.

Table 6.8: Cation % from XEDS for the different areas marked in Figure 6.10.

Area	W (cat%)	Al (cat%)	Ti (cat%)
1	0.0	83.1	16.9
2	0.0	24.8	75.2
3	0.0	18.6	81.4
4	13.8	33.9	52.3
5	5.1	12.8	82.1
6	0.0	15.5	84.5
7	0.0	10.0	90.0

Al-rich phases

In Figure 6.11 some Al-rich phases are marked. They generally appear with darker contrast than the surrounding Ti-rich phases. The Al-rich phase marked 1 in Figure 6.11 is close to a large cBN grain. The area marked with 2 and 3 seem to form a structure of light grey bubbles in a dark grey surrounding. In this area the XEDS gave a B signal as well. Area 4 has as dark
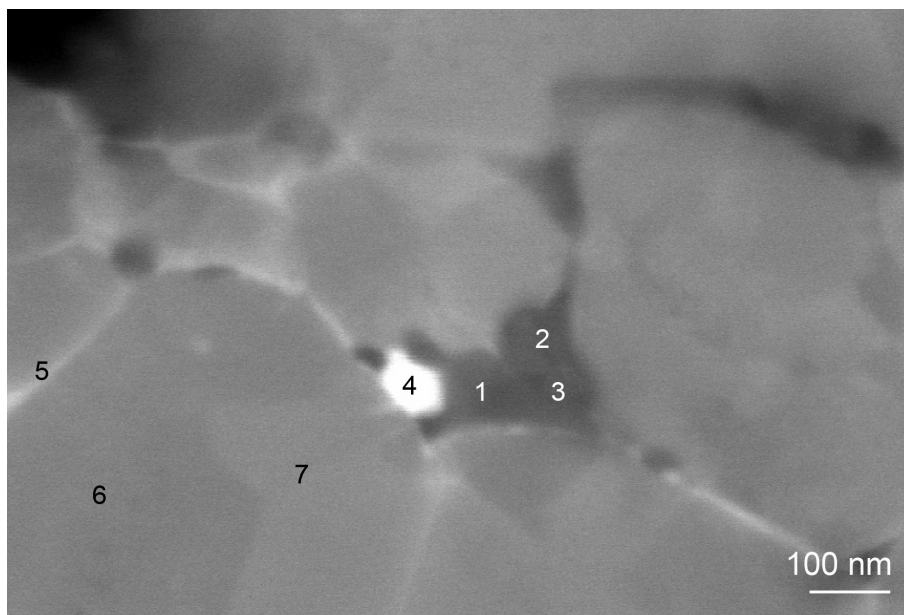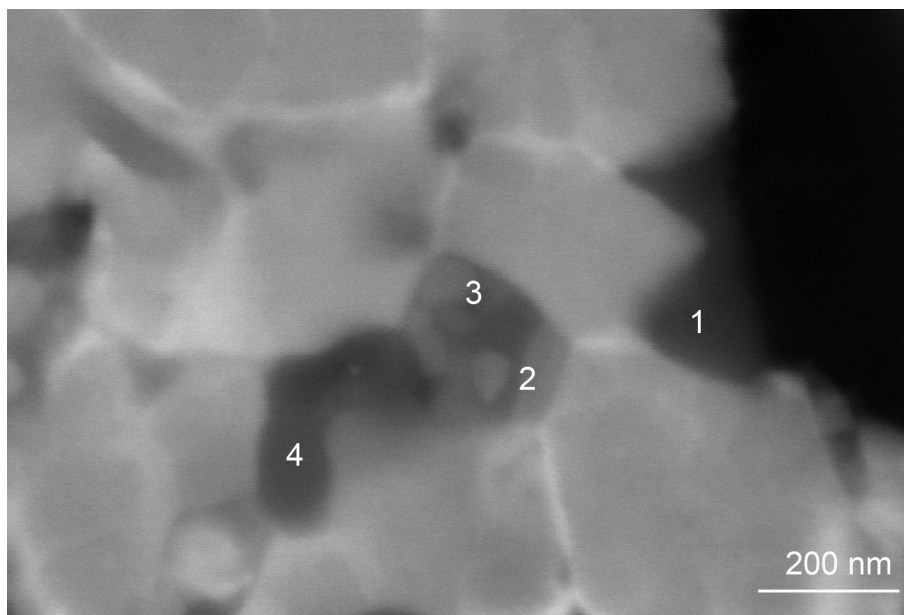
Figure 6.11: HPHT sintered material 4 (6.1 wt% Al, 3.2 wt% W, 0.3 wt% Co). XEDS for the marked areas are found in Table 6.9.

Table 6.9: Cation % from XEDS for the different areas in material 4 marked in Figure 6.11.

Area	W (cat%)	Al (cat%)	Ti (cat%)
1	0.0	72.1	27.9
2	3.5	44.0	52.5
3	0.0	61.1	38.9
4	1.1	75.8	23.1

contrast as area 1 and a very similar chemical composition with a large amount of Al.

In Figure 6.12(a) the Ti-rich grains and the white W-rich grain boundary phase are visible. The interesting feature in this material (material 4 (6.1 wt% Al, 3.2 wt% W, 0.3 wt% Co)) is the larger and darker grains present. This grain contains 100 cation % Al according to XEDS. This type of large, round, Al-rich grain are only found in materials 1 and 4. Another interesting region is shown in Figure 6.12(b). Some Al-rich grains are present in the white W-rich binding phase between two Ti-rich grains.

W-rich phases

Larger areas of brighter contrast in two materials (3 (2.9 wt% Al, 10.4 wt% W, 0.8 wt% Co) and 4 (6.1 wt% Al, 3.2 wt% W, 0.3 wt% Co)) are displayed in Figure 6.13. At a first glance
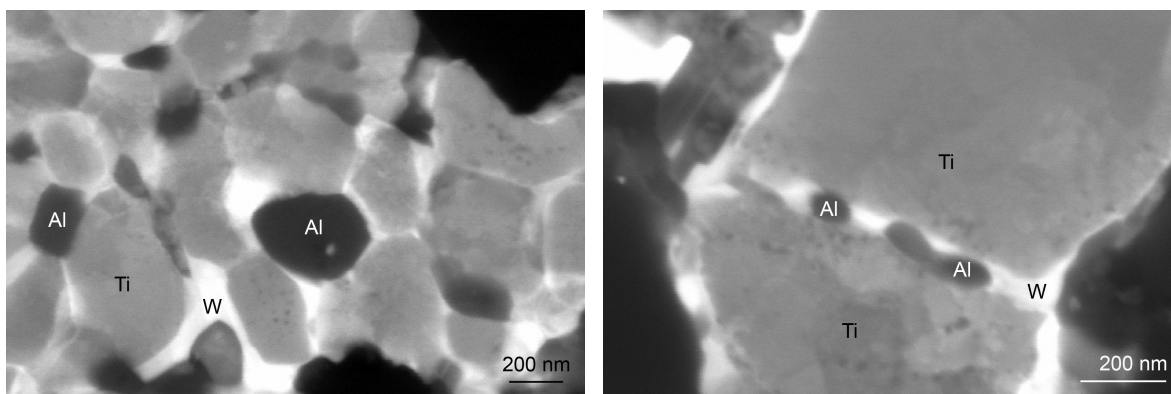
(a) Material 4 (6.1 wt% Al, 3.2 wt% W, 0.3 wt% Co).   (b) Material 5 (5.6 wt% Al, 6.5 wt% W, 0.6 wt% Co).

Figure 6.12: The dark grey areas are Al-rich phases. W- and Ti-rich phases are marked as well.

the areas in (a) and (c) look similar, but when the contrast and brightness are decreased ((b) and (d)) it is possible to distinguish a grain structure in material 4 (in (d)), but not in material 3, in (b). XEDS analysis also gives different compositions for the two cases. The white area in Figure 6.13(b) contain 100 cation % W. It also contain C. XEDS of the white area in material 4, Figure 6.13(c), gives another result. Here, also Ti was detected. The composition is different in different white grains in this micrograph. The amount of Al varies from 0 up to 35 cation % and the W to Ti cation ratio varies from 0.5 to 1.3.

Some effort was put into finding the Co in the structure. The XRD suggested the structure W_2CoB_2, so bright areas (indicating the presence of W) were extra carefully investigated. In material 6 (5.5 wt% Al, 10.3 wt% W, 0.7 wt% Co) some Co was found, in a W-rich area. An example of this can be seen in Figure 6.14. In the grains with bright contrast in this image, the number of W atoms are about twice the amount of Co. The XEDS gave 50 cation % W and 22 cation % Co in the larger white area marked 1 and 22 cation % W and 11 cation % Co in the smaller one, marked 2. The remaining cations are Al. The dark contrast surroundings contain mostly Al as cation. The Al is surrounded by black cBN grains, marked in the figure.
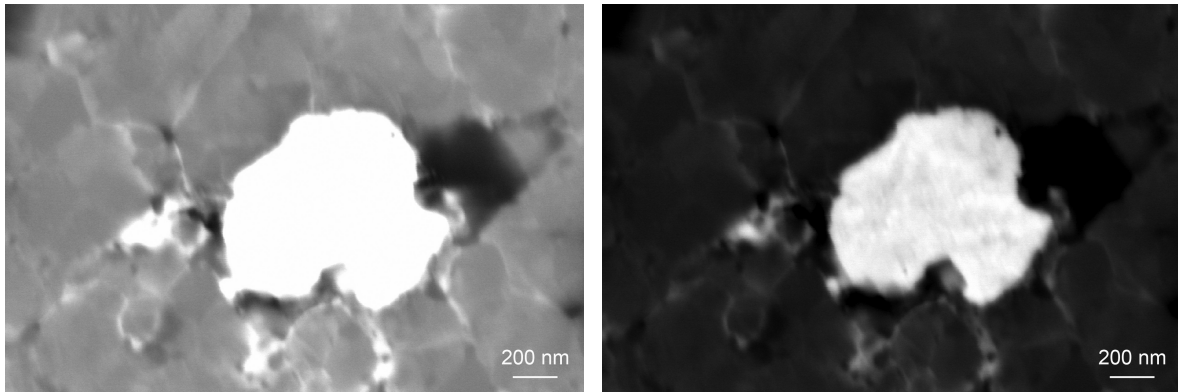
(a) Material 3 (2.9 wt% Al, 10.4 wt% W, 0.8 wt% Co). (b) Material 3 (2.9 wt% Al, 10.4 wt% W, 0.8 wt% Co), lower contrast and brightness.
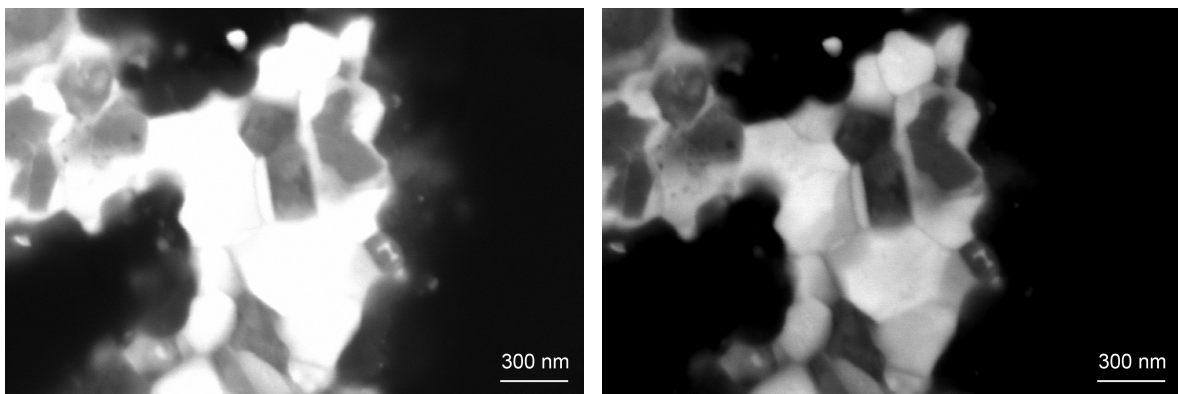
(c) Material 4 (6.1 wt% Al, 3.2 wt% W, 0.3 wt% Co). (d) Material 4 (6.1 wt% Al, 3.2 wt% W, 0.3 wt% Co), lower contrast and brightness.

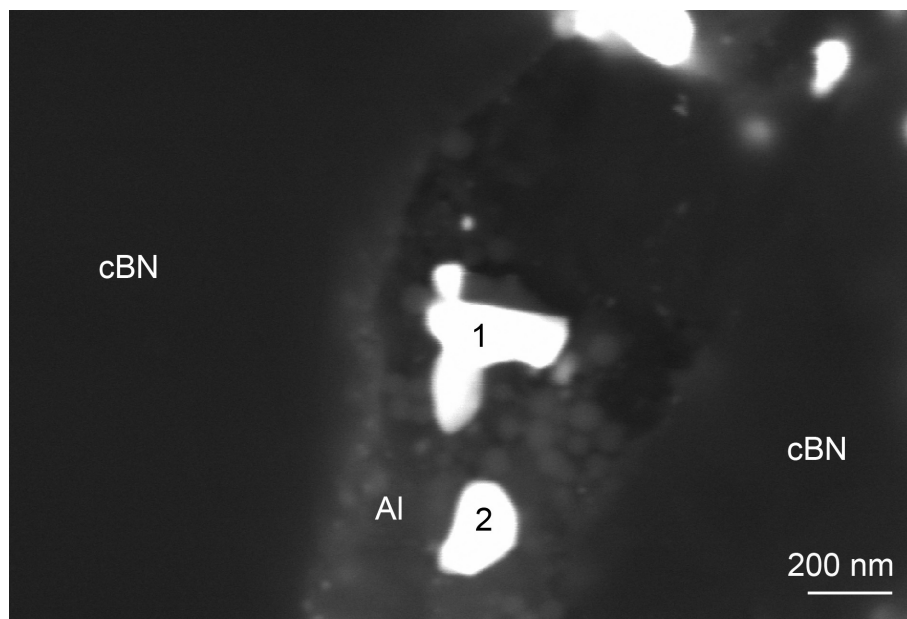**Figure 6.13:** Two different types of W-rich areas in the WC-Co milled materials.

Figure 6.14:   HPHT sintered material 6 (5.5 wt% Al, 10.3 wt% W, 0.7 wt% Co). Co is present in the white phase, marked 1 and 2, that also contain W. This phase is surrounded by dark grey Al-rich phase and black cBN grains.

6.2 Cermet milled materials

The cermet milled materials show a very interesting behaviour, though very complex.

6.2.1 Chemical analysis

For this type of milling bodies the chemical compositions evaluated by the chemical analysis are shown in Table 6.10. The results from the determination of the specific powder particle surface area are displayed in Table 6.11.

Table 6.10: Chemical composition of starting powder mixtures of the cermet milled materials in weight percentages from the chemical analysis. The amount of B is not measured in those analyses. * means that the chemical analysis was done after the pre sintering.

Material	Al (wt%)	W (wt%)	Co (wt%)	Ti (wt%)	C (wt%)	N (wt%)	O (wt%)
7	2.5	4.1	3.4	40.1	7.47	23.7	3.01
8	2.0	5.9	5.4	37.1	7.01	24.1	2.65
9	1.3	8.1	7.5	31.6	5.90	26.4	2.16
10	4.9	3.2	3.0	37.8	7.18	24.4	2.99
11	3.9	5.7	5.2	34.5	6.41	26.3	2.60
12	2.5*	8.5*	7.8*	30.4*	5.51*	26.5*	2.36*

Table 6.11: The specific surface area of the cermet milled starting powders together with the milling times. A higher area means smaller grains. * means that the milling was done at 200 rpm instead of 300 rpm and hence have a longer milling time. ** means that the specific area for this material is not measured since the chemical analysis was done after pre sintering.

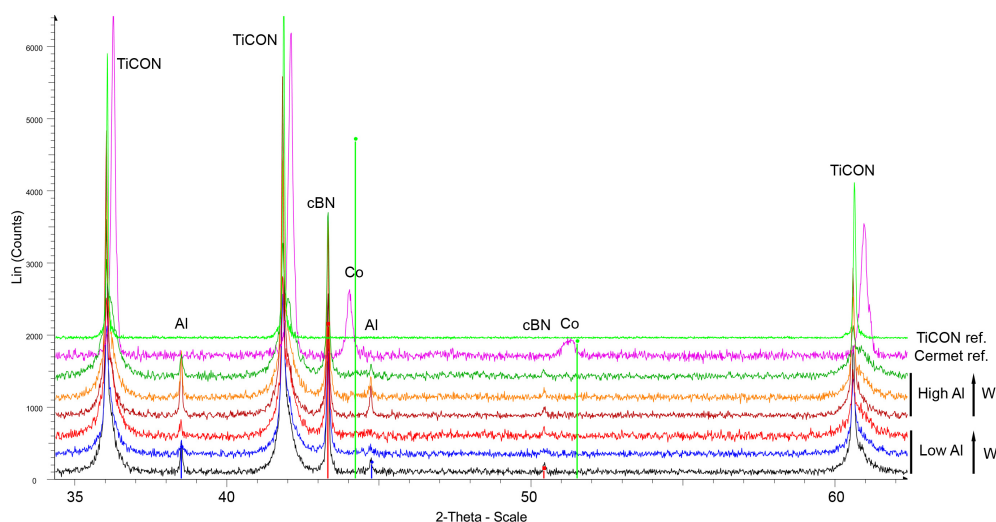| Material	Specific area (m^2/g)	Pre milling time	Milling time
7	7.55	12 h*	5 h*
8	7.45	8 h	6 h 25 min
9	8.04	8 h	10 h 20 min
10	6.99	8 h	2 h 40 min
11	7.40	8 h	6 h 25 min
12	**	8 h	10 h 20 min

Figure 6.15: XRD spectra before sintering for materials 7-12. On top there is a TiCON raw material reference spectrum and a cermet milling body reference spectrum.

6.2.2 XRD

The XRD spectra for the cermet-milled materials (7-12) are shown in Figures 6.15, 6.16 and 6.17. These spectra are adjusted in 2θ according to the cBN peaks in the same way as the spectra for the WC-Co milled materials.

First, the XRD spectra before sintering are considered, seen in Figure 6.15. In these spectra the raw materials, cBN, Ti(C,O,N) and Al are visible. The magenta spectrum is the cermet milling body reference. This could be off shifted in 2θ, just like the Ti(C,O,N) reference since I do not have any reference peaks. The cermet contains (Ti,W)(C,N) and Co. These two phases are visible in the spectrum. The Co is slightly shifted to the left from the data base values (green markers). This might be due to small amounts of other elements being dissolved in the Co binder phase. It might also be the entire spectrum that is shifted since I do not have a reference. The (Ti,W)(C,N) peaks are shifted compared to the Ti(C,O,N) peaks of the raw material powder as well. This is probably due to the W and absence of O in the structure, giving a different lattice parameter to the milling body. The Co and (Ti,W)(C,N) peaks are quite wide, which might indicate that the stoichiometry of the phases is varying. The Co is not visible in the spectra of material 7 to 12.

For the pre sintered and HPHT sintered materials the phases identified in the spectra are displayed in Tables 6.12 and 6.13. cBN, Ti(C,O,N) and AlCo are present in all pre sintered materials, and Co in all except materials 10 (4.9 wt% Al, 3.2 wt% W, 3.0 wt% Co) and 11 (3.9 wt% Al, 5.7 wt% W, 5.2 wt% Co). The HPHT sintered materials contain all cBN and Ti(C,O,N) and an unidentified peak at 45.6 °. The spectrum of material 10 also contain TiB_2, Al_2O_3 and another unidentified peak at 44.6 °.
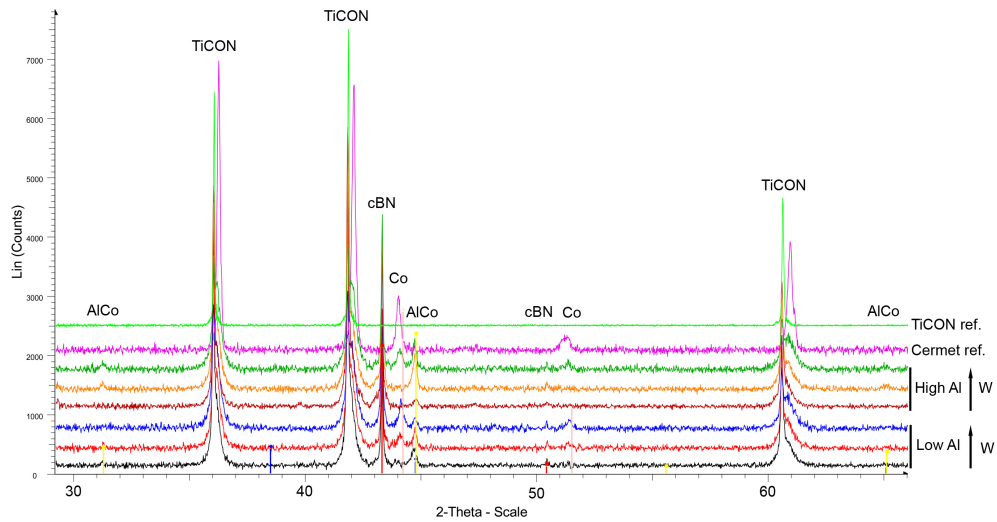
Figure 6.16: XRD spectra for pre sintered materials 7-12.
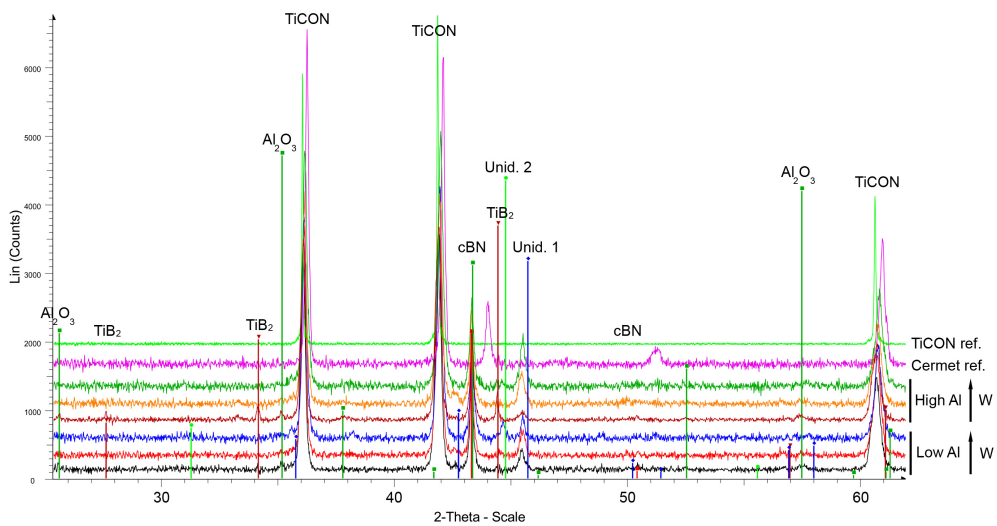
Figure 6.17: XRD spectra for HPHT sintered materials 7-12. Unid. 1 and Unid. 2 are peaks that have not been identified.

Table 6.12: The amount of Al, Co and W from chemical analysis and the phases present in the XRD spectra after pre sintering for materials 7-12. * means that the chemical analysis was done after the pre sintering.

Material	Al (wt%)	W (wt%)	Co (wt%)	Phases
7	2.5	4.1	3.4	cBN, Ti(C,O,N), AlCo, Co
8	2.0	5.9	5.4	cBN, Ti(C,O,N), AlCo, Co
9	1.3	8.1	7.5	cBN, Ti(C,O,N), AlCo, Co
10	4.9	3.2	3.0	cBN, Ti(C,O,N), AlCo
11	3.9	5.7	5.2	cBN, Ti(C,O,N), AlCo
12	2.5*	8.5*	7.8*	cBN, Ti(C,O,N), AlCo, Co

Table 6.13: The amount of Al, Co and W from chemical analysis and the phases present in the XRD spectra after HPHT sintering for materials 7-12. * means that the chemical analysis was done after the pre sintering. The unidentified phases only have one peak present and thus the identification of those are uncertain.

Material	Al (wt%)	W (wt%)	Co (wt%)	Major phases	Unidentified phases: 2θ (°); d (Å)
7	2.5	4.1	3.4	cBN, Ti(C,O,N)	45.6; 1.988
8	2.0	5.9	5.4	cBN, Ti(C,O,N)	45.6; 1.988
9	1.3	8.1	7.5	cBN, Ti(C,O,N)	45.6; 1.988, 44.6; 2.030
10	4.9	3.2	3.0	cBN, Ti(C,O,N), TiB$_2$, Al$_2$O$_3$	45.6; 1.988
11	3.9	5.7	5.2	cBN, Ti(C,O,N)	45.6; 1.988
12	2.5*	8.5*	7.8*	cBN, Ti(C,O,N)	45.6; 1.988

Ti(C,O,N) lattice parameters

In Figure 6.18 the Ti(C,O,N) 200 peak for material 12 (2.5 wt% Al, 8.5 wt% W, 7.8 wt% Co) can be seen before sintering, after pre sintering and after HPHT sintering. Before sintering the peak consists of one narrow peak and a wider shoulder on the right side. The high, narrow peak originates from the initial Ti(C,O,N) raw material powder. The shoulder comes from the cermet milling body. After pre sintering the peak has not changed shape that much. However, something happed during the HPHT sintering, that changed the structure of the Ti(C,O,N). The peak does not only shift, but it also gets wider and change shape. The shoulder from the milling debris disappear completely.

By the use of equation (3.2) the lattice parameters were calculated for these materials as well. The 2θ value of the high, narrow peaks were used, marked by arrows in the figure. The results are shown in Table 6.14. Again, no clear change can be seen during pre sintering. After HPHT sintering however, the lattice parameter was reduced and appeared to be dependent on the milling time. A longer milling time had resulted in an even more reduced lattice parameter. It is worth noting that the more milling debris, the closer the peaks get to the milling body peaks.
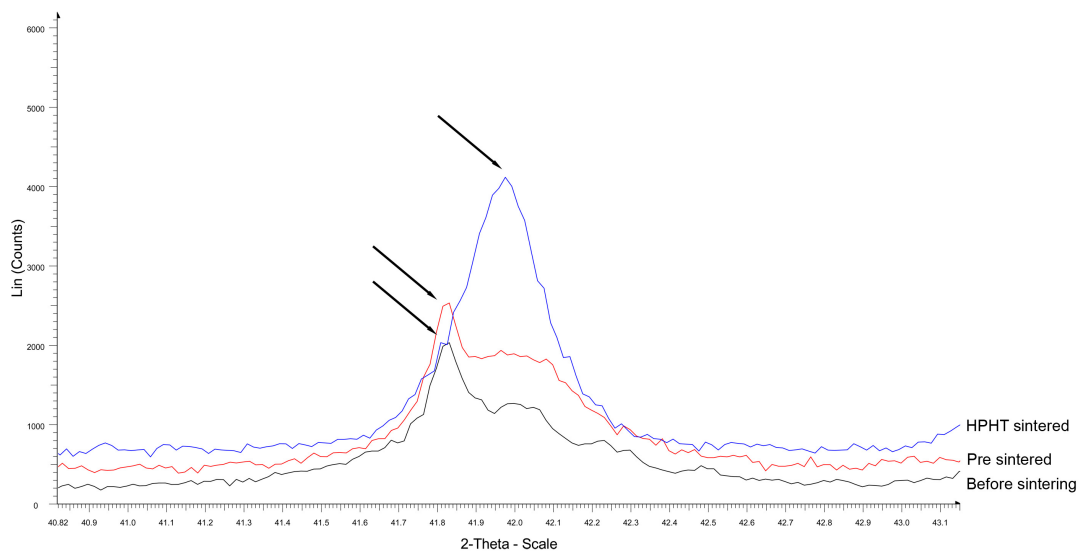

Figure 6.18: The Ti(C,O,N) 200 peak from material 12 (2.5 wt% Al, 8.5 wt% W, 7.8 wt% Co). The black spectrum is taken before sintering, the red is from the pre sintered and the blue from the HPHT sintered material. The arrows mark the positions of the 200 peaks that have been used for the calculations in Table 6.14.

Table 6.14: Lattice parameters during the process for the cermet milled materials.

Material	a before (Å)	a pre sint. (Å)	a HPHT sint. (Å)
7	4.317	4.317	4.310
8	4.317	4.317	4.307
9	4.317	4.318	4.305
10	4.317	4.317	4.310
11	4.317	4.317	4.306
12	4.317	4.317	4.302

6.2.3 SEM and XEDS of the pre sintered materials

Overviews of materials 7 (2.5 wt% Al, 4.1 wt% W, 3.4 wt% Co) and 12 (2.5 wt% Al, 8.5 wt% W, 7.8 wt% Co) are shown in Figures 6.19 and 6.20. Again, the imaged surfaces of the pre sintered materials are fracture surfaces. The pre sintered materials are porous and thus the black areas might be both cBN and pores.

Higher magnifications of the same materials are shown in Figure 6.21 and 6.22. The cation % of the marked areas are displayed in Tables 6.15 and 6.16. The amount of different elements seems to vary in the materials, areas that might look similar do not always contain the same elements. W, Al, Ti and Co cations are detected.
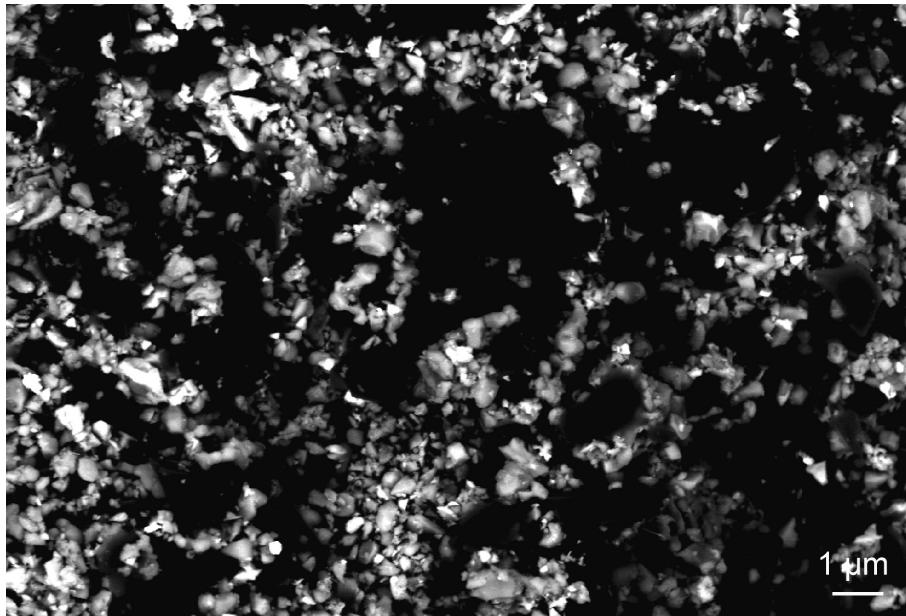
Figure 6.19: Pre sintered material 7 (2.5 wt% Al, 4.1 wt% W, 3.4 wt% Co).
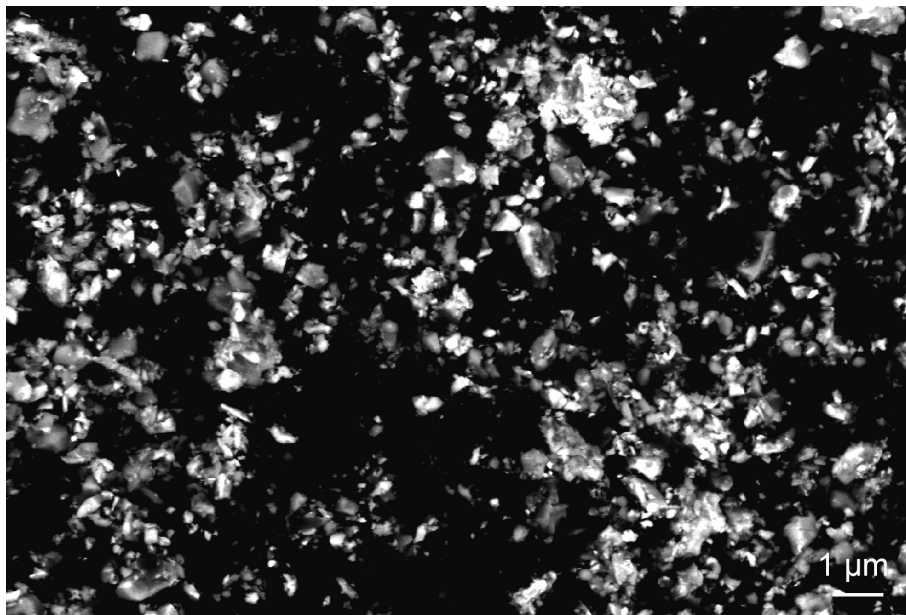
Figure 6.20: Pre sintered material 12 (2.5 wt% Al, 8.5 wt% W, 7.8 wt% Co).
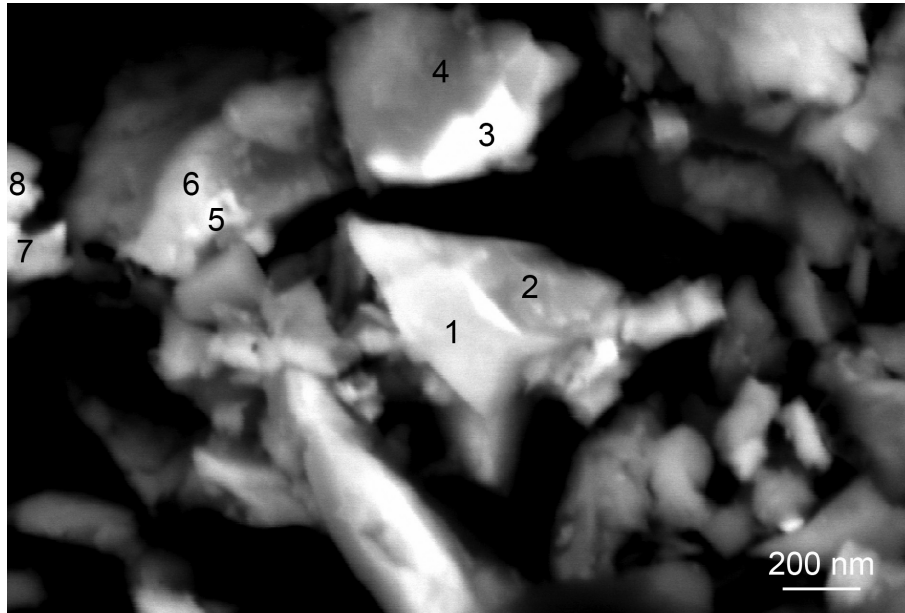
Figure 6.21: Pre sintered material 7 (2.5 wt% Al, 4.1 wt% W, 3.4 wt% Co). XEDS for the marked areas are found in Table 6.15.

Table 6.15: Cation % from XEDS for the different areas in material 7 marked in Figure 6.21.

Area	W (cat%)	Al (cat%)	Ti (cat%)	Co (cat%)
1	21.2	0.0	78.8	0.0
2	10.6	0.0	89.4	0.0
3	26.0	0.0	74.0	0.0
4	8.0	0.0	92.0	0.0
5	10.8	14.6	56.9	17.7
6	17.1	0.0	82.9	0.0
7	5.7	10.8	45.9	37.6
8	14.8	9.7	67.8	7.8
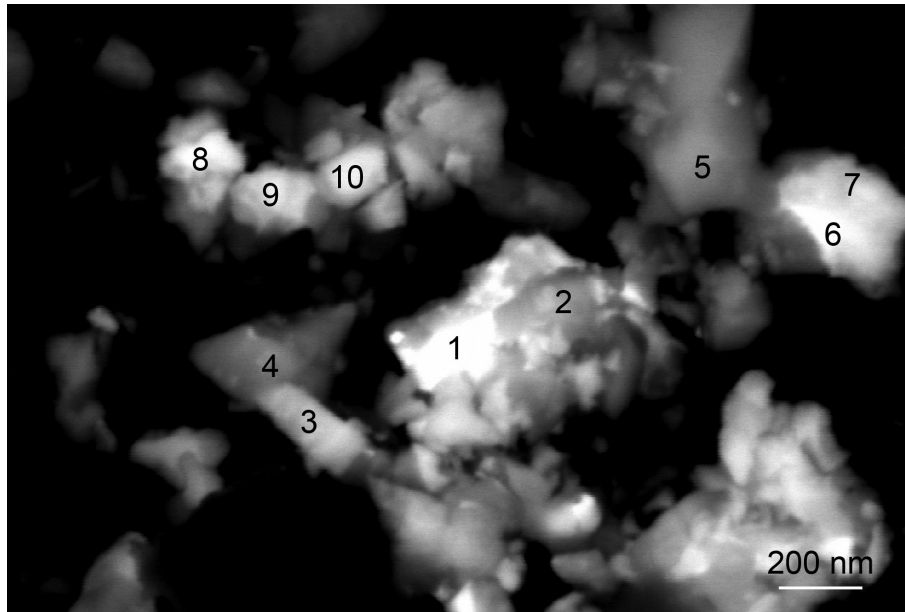
Figure 6.22: Pre sintered material 12 (2.5 wt% Al, 8.5 wt%W, 7.8 wt% Co). XEDS for the marked areas are found in Table 6.16.

Table 6.16: Cation % from XEDS for the different areas in material 12 marked in Figure 6.22.

Area	W (cat%)	Al (cat%)	Ti (cat%)	Co (cat%)
1	78.8	0.0	21.2	0.0
2	8.7	11.6	71.1	8.6
3	9.9	11.9	74.7	3.5
4	2.9	11.2	82.7	3.3
5	2.4	11.1	86.5	0.0
6	12.3	11.3	70.3	6.1
7	7.5	9.6	79.8	3.1
8	8.6	21.2	51.0	19.2
9	15.1	20.3	56.6	8.0
10	10.8	11.1	73.2	4.9

6.2.4 SEM and XEDS of the HPHT sintered materials

An overview of materials 7 to 12 after HPHT sintering is shown in Figure 6.23. The black grains are as usual cBN. Between those it is possible to distinguish some different structures. The structures look fairly different in the different materials. In the images of materials 7 (2.5 wt% Al, 4.1 wt% W, 3.4 wt% Co) and 10 (4.9 wt% Al, 3.2 wt% W, 3.0 wt% Co), it is possible to spot smaller, dark grey features. These contain Al and might be Al_2O_3. In all materials there are phases with grey contrast, and varying brightness, between the cBN grains. These are generally rich in Ti and W, and are probably a Ti(C,O,N) like structure. Some of these grains also contain varying amounts of W, Al and Co. In some materials it is also possible to spot a phase with bright contrast between the grains with grey contrast. This phase contains Co from the milling bodies. These different areas are marked in Figure 6.23(a).

Close up

Two close ups of material 8 (2.0 wt% Al, 5.9 wt% W, 5.4 wt% Co) are shown in Figure 6.24. In Table 6.17 the cation compositions of the different areas marked in Figure 6.24(a) are displayed. According to XEDS, all areas also contain C. Area 2 also gave B and N signal. This B and N signal probably comes from the close by cBN grain. The Co detected might come from the thin grain boundary film with bright contrast between the grain marked 2 and the other grey contrast grains. If this is the case, area 2 and 3 contain Ti, W and C, and are probably (Ti,W)(C,O,N). Area 1 and 4 contain W, Al, Ti, Co and C. This phase has probably formed during HPHT sintering. No phase containing all these different elements has been found in the XRD spectra.

The microstructures are very different in the two micrographs in the figure, that image two areas just a few microns apart. In most areas, the Ti-rich grains are surrounded by a Co-rich phase, which appears with bright contrast. This can be seen in Figure 6.24(b).

Figure 6.25 illustrates another type of microstructure, with varying amounts of W detected in the features with different contrasts around the central darker grain (see Table 6.18). The W signal in the central grain might come from the W-rich bright phase surrounding it.

In Figure 6.26 another example of a HPHT sintered cermet milled material is shown, this time material 9 (1.3 wt% Al, 8.1 wt% W, 7.5 wt% Co) is investigated. According to XEDS, the feature with bright contrast, marked with 1 in the figure, contains W, Al, Ti, Co and Mo, see Table 6.19. Mo was not added intentionally to the material. The Co-rich phase with bright contrast between other grains is commonly occurring in the cermet milled materials. Areas 2, 3 and 4 contain Ti and W. They are probably (Ti,W)(C,O,N) grains. The Co signal detected in area 4 might come from the close by bright contrast area.
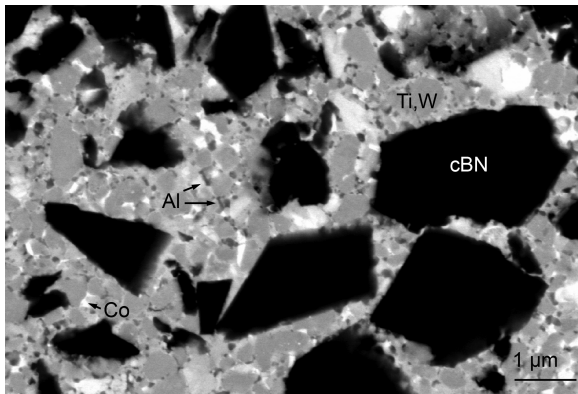
(a) Material 7 (2.5 wt% Al, 4.1 wt% W, 3.4 wt% Co)
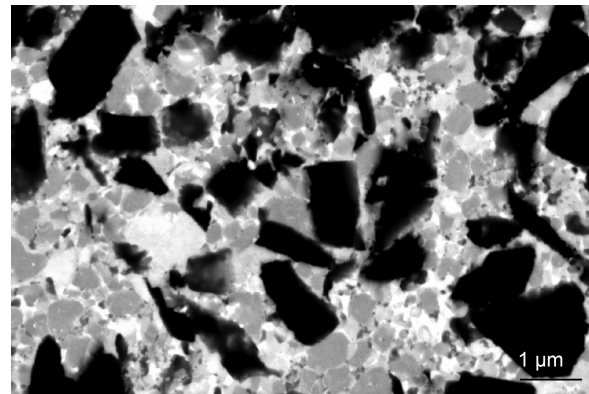
(b) Material 8 (2.0 wt% Al, 5.9 wt% W, 5.4 wt% Co)
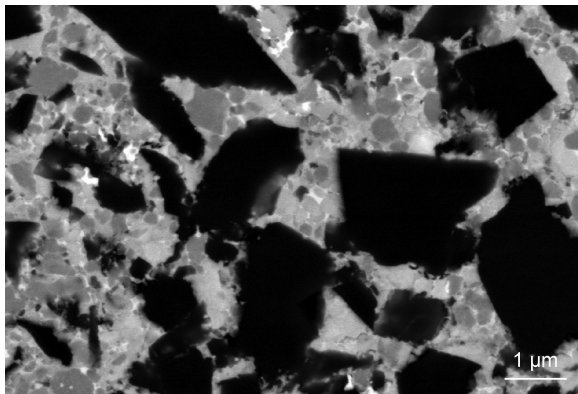
(c) Material 9 (1.3 wt% Al, 8.1 wt% W, 7.5 wt% Co)
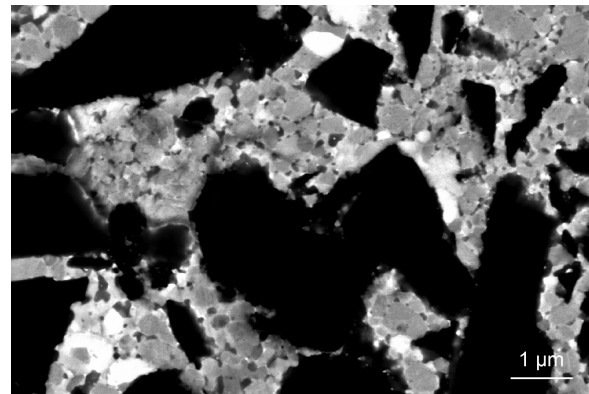
(d) Material 10 (4.9 wt% Al, 3.2 wt% W, 3.0 wt% Co)
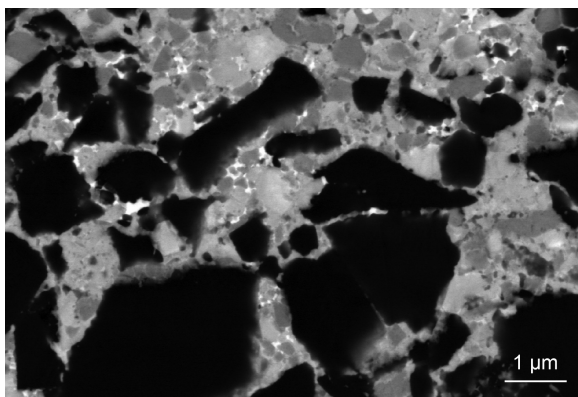
(e) Material 11 (3.9 wt% Al, 5.7 wt% W, 5.2 wt% Co)
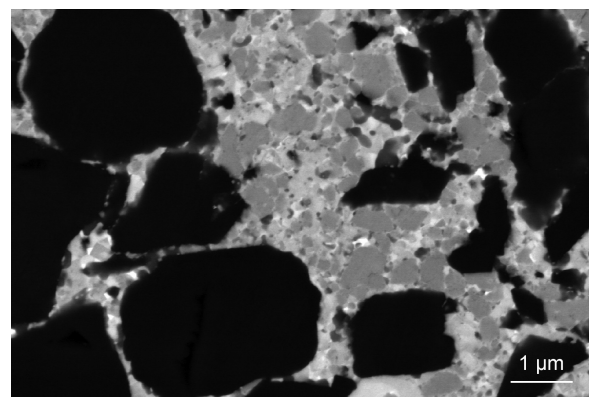
(f) Material 12 (2.5 wt% Al, 8.5 wt% W, 7.8 wt% Co)

Figure 6.23: Overview of all the HPHT sintered cermet milled materials. The black areas are cBN and dark grey small features is Al-rich. Light grey generally contain Ti, W or Co or all of them. White contrast between Ti-rich grains contain Co. The different ares are marked in (a).
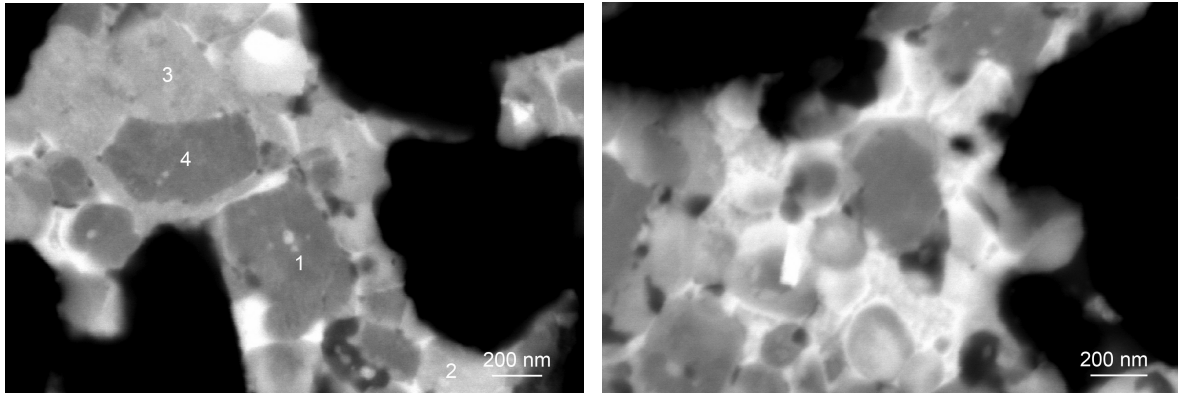
(a) Material 8 (2.0 wt% Al, 5.9 wt% W, 5.4 wt% Co), (b) Material 8 (2.0 wt% Al, 5.9 wt% W, 5.4 wt% Co).
HPHT sintered. The composition of cations for area The white structure contains different amounts of Co.
1-4 is shown in Table 6.17.

Figure 6.24: Two examples of the local microstructure in material 8.

Table 6.17: Cation % from XEDS for the different areas in material 8 marked in Figure 6.24(a).

Area	W (cat%)	Al (cat%)	Ti (cat%)	Co (cat%)
1	4.3	14.6	73.3	7.7
2	18.6	0.0	69.5	12.0
3	12.9	0.0	87.1	0.0
4	4.1	14.6	76.3	5.0
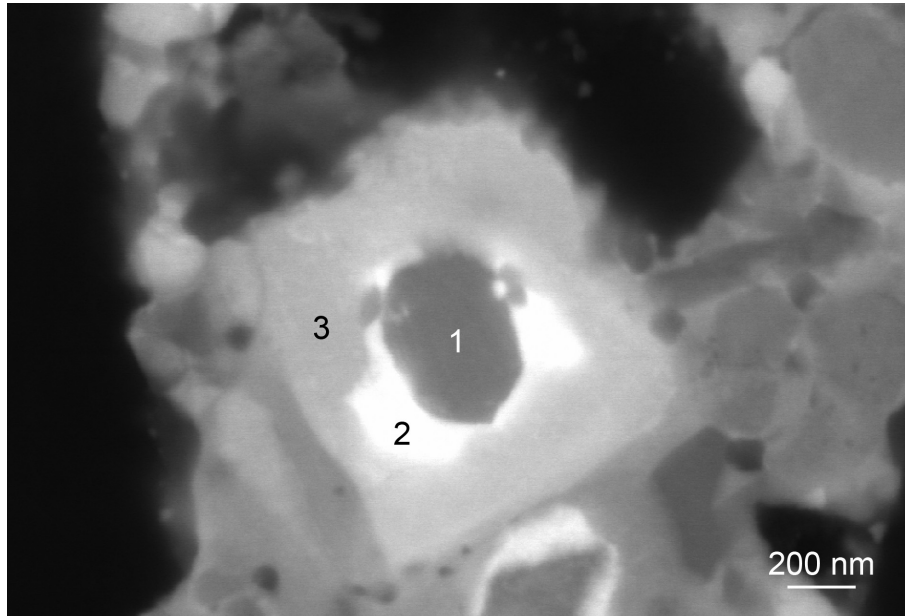
Figure 6.25: Material 10 (4.9 wt% Al, 3.2 wt% W, 3.0 wt% Co). The different contrasts marked with 1, 2 and 3 correspond to different amounts of W, given in Table 6.18.

Table 6.18: Cation % from XEDS for the different areas in material 10 marked in Figure 6.25.

Area	W (cat%)	Al (cat%)	Ti (cat%)
1	7.7	0.0	92.3
2	18.9	0.0	81.1
3	8.5	3.3	88.2
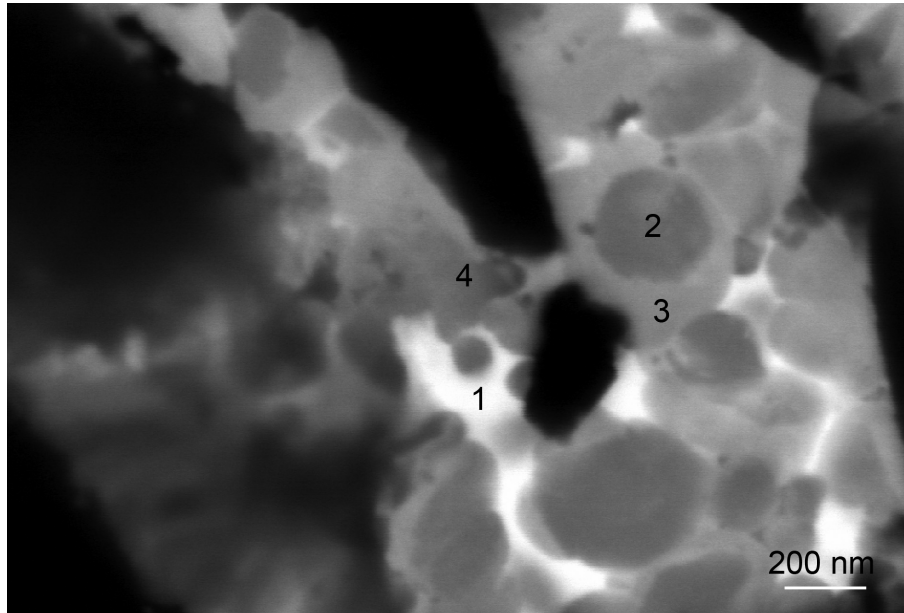
Figure 6.26: Material 9 (1.3 wt% Al, 8.1 wt% W, 7.5 wt% Co). XEDS cation % for the marked areas are given in Table 6.19.

Table 6.19: Cation % from XEDS for the different areas in material 9 marked in Figure 6.26.

Area	W (cat%)	Al (cat%)	Ti (cat%)	Co (cat%)	Mo (cat%)
1	7.2	9.7	24.9	26.6	31.6
2	9.6	0.0	90.4	0.0	0.0
3	11.6	0.0	88.4	0.0	0.0
4	4.0	0.0	92.1	3.9	0.0
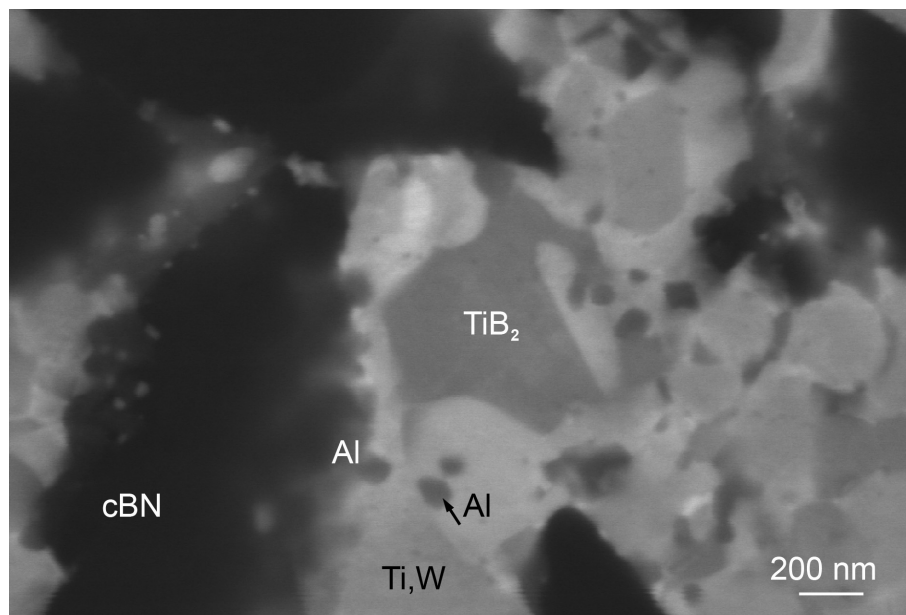
Figure 6.27: HPHT sintered material 10 (4.9 wt% Al, 3.2 wt% W, 3.0 wt% Co). The large grey area in the middle contain Ti and B according to XEDS.

Ti- and B-containing area

Figure 6.27 illustrates a larger area containing Ti and B. This material, material 10 (4.9 wt% Al, 3.2 wt% W, 3.0 wt% Co), was the only one where these kinds of quite large Ti- and B-containing areas could be found. According to XRD this material contain TiB_2. The area is much larger than the TiB_2 grains in the WC-Co milled materials. The big grains with black contrast are cBN. Close to the edges of the cBN grains there is an Al-rich phase with dark grey contrast. An Al-rich smaller feature is also marked in the figure. A Ti-rich phase containing some W is surrounding the TiB_2 area.

Al-rich grain boundary film

An example of an Al-rich grain boundary film found in material 12 (2.5 wt% Al, 8.5 wt% W, 7.8 wt% Co) is shown in Figure 6.28. The film is marked by arrows in the figure. The boundary film is very thin, between two Ti- and W-containing grains marked 2 and 3. Closest to the cBN grain with black contrast it has a triangular shape. Table 6.20 contain XEDS for areas 1 to 5. The smaller a feature investigated with XEDS is, the more signal might come from areas beside or under the feature of interest. The areas marked 1, 2 and 3 are very close to each other and to other features, and thus the signals from different phases might mix. The area marked 4 contain more W than areas 2 and 3. Area 5 is rich in both Ti and Al.
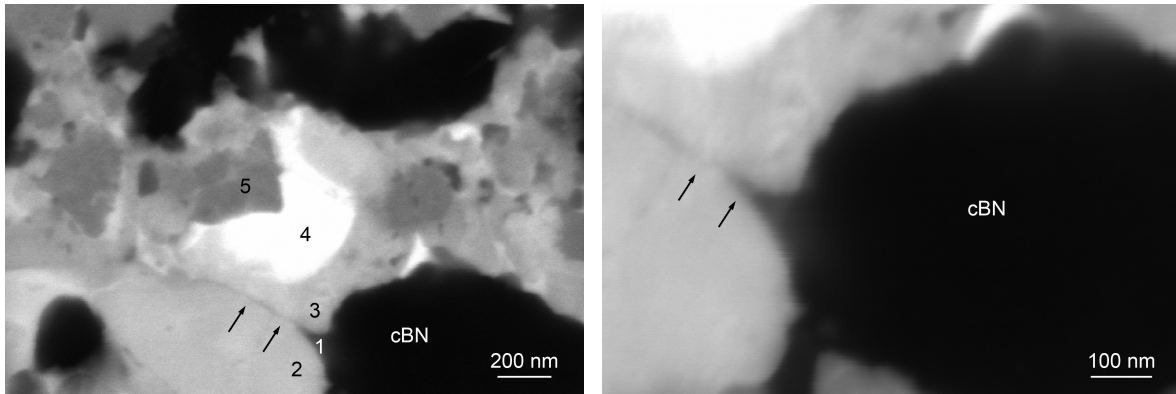
(a) Material 12. XEDS for the marked areas are found in Table 6.20.

(b) Material 12. Magnification of the Al-rich grain boundary film in (a).

Figure 6.28: Al-rich grain boundary film in material 12 (2.5 wt% Al, 8.5 wt% W, 7.8 wt% Co). Note the dark grain boundary between two light grey grains marked with arrows.

Table 6.20: Cation % from XEDS for the different areas in material 12 marked in Figure 6.28(a).

Area	W (cat%)	Al (cat%)	Ti (cat%)	Co (cat%)
1	4.5	68.6	23.7	3.2
2	18.7	9.1	72.2	0.0
3	18.8	32.1	44.0	5.2
4	53.4	0.0	46.6	0.0
5	7.2	24.9	61.7	6.2

7

Discussion

Here the data from the results chapter are further discussed and interpreted. The different phases are discussed separately for the two types of milling bodies.

7.1 WC-Co milled materials

Again the WC-Co milled materials are discussed first.

7.1.1 Powder characterisation

The results from the chemical analysis, Table 6.1, seem to match the test plan quite well. The specific surface area in Table 6.2 is dependent on milling time, the longer milling time the larger area, indicating smaller particles. The cBN grains are so hard that their grain size is probably not affected during milling, they rather contribute to milling the milling bodies themselves. It is more likely that the Ti(C,O,N) powder is milled into smaller particles. The mill debris from the milling bodies might also contribute to the increased surface area.

7.1.2 Phase composition

Both after pre sintering and after HPHT sintering new phases were created. Here, they are discussed. Both SEM, XEDS and XRD results are put together.

Ti(C,O,N)

The Ti(C,O,N) lattice parameters are unchanged during the pre sintering, as seen in Table 6.5. There are light grey grains in the images of the microstructure of the pre sintered material, seen in Figure 6.7, areas 3, 4, 8 and 9, and in Figure 6.8, areas 4 and 5. The areas are identified as Ti(C,O,N), since the largest amount of cation found in this type of area is Ti. The Ti(C,O,N) particles seem to have started forming a network of sintered particles. The edges of the particles

Table 7.1: Lattice parameters for different Ti(C,O,N), values from [16].

Compound	lattice parameter (Å)
TiN	4.242
$TiC_{0.3}N_{0.7}$	4.264
$TiC_{0.7}N_{0.3}$	4.297
$TiC_{0.53}N_{0.32}O_{0.19}$	4.300
TiC	4.327

are quite round and the grains have formed necks between them. The arrow in Figure 6.7(a) marks this kind of structure. The three grains have formed necks between each other and fill out the space between them.

Al is detected with XEDS in all areas marked in the figure, Figure 6.7. The Ti(C,O,N) raw material powder does not contain Al from the start, so the question is in what form the Al found on the grains might be. The Al might have become a part of the Ti(C,O,N) structure. However, the Ti(C,O,N) peaks in the XRD spectra did not change shape during the pre sintering, something that would occur when the composition of a phase is changed. Another possibility is that the Al might be located on the surface, as a thin grain boundary film, in too small amounts to be detected with XRD.

During HPHT sintering the lattice parameter of Ti(C,O,N) changes, and gets larger, see Table 6.5. This would be due to a change in the chemical composition of the phase during the HPHT sintering. The O in the Al_2O_3 that appears in the XRD spectra during HPHT sintering is supposed to be taken from the Ti(C,O,N) and the surface oxides of the raw material powders. The amount of Al is calculated such that all O will react with Al. Thus, it is probably less or no O in the Ti(C,O,N) grains after HPHT sintering. In the following text Ti(C,O,N) is used even though it is not entirely sure wether there is any O in these grains or not. According to XEDS there is usually C, but no O.

Table 7.1 contains lattice parameter values for different stoichiometries of Ti(C,O,N) taken from [16] for comparison. The lattice parameter is dependent on the amount of C, N and O in the Ti(C,O,N). When comparing only the values for the Ti(C,N) without O, the trend is increased lattice parameter for higher amounts of C. The increase in lattice parameter during HPHT sintering might imply that the Ti(C,O,N) phase get more similar to TiC. The amount of N was very small compared to the amount of C in the raw material starting powder, and during the entire process the lattice parameter is much closer to TiC than TiN.

The shape of the peak also changes during HPHT sintering. It gets both broader and lower. The broadening of the peak might depend on a varying composition of the phase. Some more Ti-C-O-N compositions than before might be present, possibly with more elements in the structure. Al is detected when analysing the Ti-rich phase, in Figure 6.10. The Al might be dissolved in the Ti(C,O,N).

Both W and Ti are found in some bright contrast grains in Figure 6.13(d). The shape of the
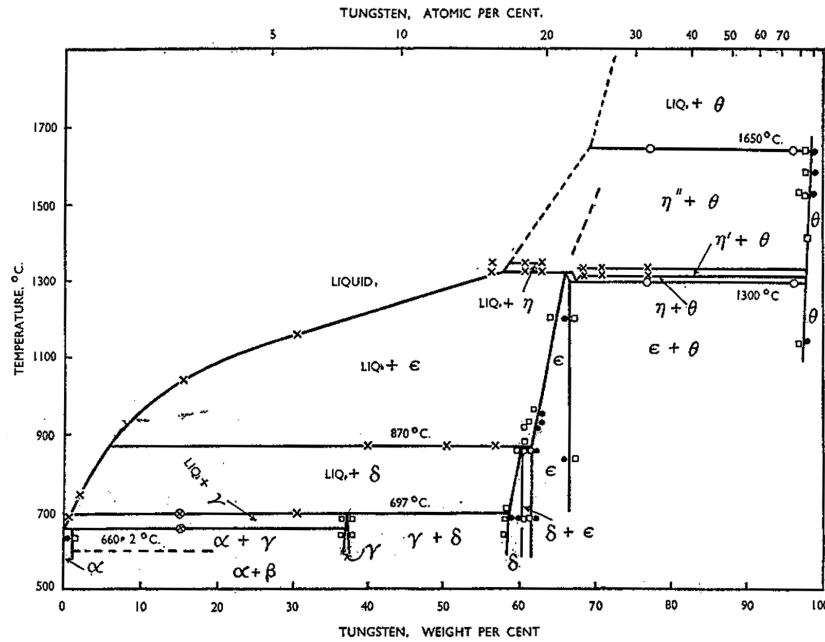
Figure 7.1: The Al-W phase diagram, taken from [17]. ϵ in the diagram is Al_4W, δ is Al_5W and γ is $Al_{12}W$.

grains, straight edges and round shapes, makes it more probable that these have formed during sintering rather than being remainders from earlier reactions or raw materials. This might be some kind of (Ti,W)(C,N) structure, formed from a Ti- and W-rich liquid during cooling. (Ti,W)(C,N) have the same structure as Ti(C,N), but another lattice parameter. This should therefore not give new peaks in the XRD spectra, but a broadening in the already existing Ti(C,N) peaks due to a more varied stoichiometry. This could also explain the absence of W-containing phases in the XRD from some of the materials. The W content could be hidden in the Ti(C,O,N) peak.

Al- and W- containing phases

During the pre sintering the phases start to react and create new phases as seen in Figure 6.2. The metallic Al is gone and it seems to have reacted with some of the WC to form Al_4W and Al_5W. It is interesting to note that in only one of the materials, material 4, Al_5W is formed instead of Al_4W. Though, it is not surprising that the one with the high amount of Al and the low amount of W is the one that contains Al_5W instead of Al_4W if any of the materials did. According to a phase diagram of Al and W, Figure 7.1, some different phases are possible: Al_4W, Al_5W and $Al_{12}W$ to mention three. Al_4W would exist in equilibrium with and Al liquid containing around 7 wt% W at 900 °C, the pre sintering temperature. The three Al-W phases all occur at temperatures under 900 °C. Thus they might all form during the cooling.

Areas 1, 2 and 5 in the micrograph of material 4, in Figure 6.7, has a Al:W ratio of approxi-

mately 10. This suggests the presence of $Al_{12}W$. $Al_{12}W$ was not detected with XRD but might still be there in small amounts, again according to the phase diagram in Figure 7.1. The other W- and Al- containing areas, 6 and 7, have a Al:W ratio of down to approximately 7 and might be Al_5W.

The Al-W-phases were created in separate locations in the microstructure, possibly where the W of the milling bodies was available. Thus there are probably local variations in the amount of Al atoms close to W atoms. The Al-W phases have started to form networks between the light grey Ti-rich grains. The shape of this phase makes it probable that the Al-W phases has been liquid during the pre sintering, which is possible according to the phase diagram.

During the HPHT sintering the temperature is increased up to $1400\,°C$. According to the phase diagram, the Al-W phases may become liquid at this temperature. The Al and W may react with other elements, since there seems to be no Al-W phases left after HPHT sintering. The Al and W form other phases; Al_2O_3, AlN, (Ti,W)(C,O,N), W_2CoB_2 and W-rich grain boundary films.

WC

After pre sintering WC is still found in materials 2, 3 and 6. Area 1 and 2 in Figure 6.8 (material 6) contain around 80 cation % W and 20 cation % Al according to the XEDS. Thus, this is a too small amount of Al for being Al_4W or Al_5W. More probable is that this is WC, with Al in the close surroundings or on the surface. The WC should come directly from the milling bodies and that would explain the sharp and edgy corners of the bright area.

After HPHT sintering the only materials containing WC according to XRD are materials 2 and 3. Thus, the WC in material 6 have reacted and formed other phases, possibly contributing to the W in the W_2CoB_2, the (Ti,W)(C,O,N) or in the W-rich grain boundary film.

Figure 6.13(b) reveals a structure containing W. The only cation found is W. Except for W, C was also detected in the structure. According to XRD the only phase containing W cations in material 3 is WC. The irregular shape of the area suggests that the WC comes from the milling body.

Al_2O_3, AlN and TiB_2

After pre sintering the Al seems to be either in the shape of Al_4W, Al_5W or $Al_{12}W$, or on the surfaces of Ti(C,O,N) grains, as discussed above. However, there are two different Al-rich phases after HPHT sintering. According to XRD there is both Al_2O_3 and AlN, see Table 6.4.

The reason for putting Al_2O_3, AlN and TiB_2 under the same heading is that they are found close to each other and sometimes they are hard to distinguish from each other. If Al and O is found close to both a cBN grain and a Ti(C,O,N) grain, all of Al, O, B, N, Ti and C might be detected with XEDS. Then, it is not possible to know if there is only Al_2O_3, or maybe all three Al_2O_3, AlN and TiB_2. The phases generally seem to appear close to each other.

Area 1 in Figure 6.11 is Al-rich (and contains some Ti, probably from the surroundings). It is situated close to a cBN grain, a quite common location for Al-rich phases. It might be AlN or Al_2O_3. The areas marked 2 and 3 in Figure 6.11 contain according to XEDS both Al, Ti and B. This together with the slightly darker contrast than the Ti(C,N) grains makes it possible

that this area might contain some of the TiB_2 detected in the XRD analysis. The shape, of brighter bubbles inside the darker Al-rich phase, is worth noting. This kind of structure might occur when a new phase is forming, and the growth process is interupted before it has finished by the limited sintering time.

The Al-rich area in Figure 6.12(a) contains only Al as cation. There is an O peak in the XEDS spectra, so it is Al_2O_3 rather than AlN. This grain is fairly large and round for being an Al-rich feature.

Grain boundaries

In the HPHT sintered materials one type of grain boundary film were found. This is the bright phase, marked 5 in Figure 6.10. This contain more W than the surrounding Ti(C,O,N) grains. However, the composition of this phase is impossible to decide with the techniques used since it is too thin. This kind of thin film between the other grains suggests that the phase has been liquid during the HPHT sintering. The W might come from the Al-W networks that was present after pre sintering.

W_2CoB_2

In the pre sintered materials no Co-containing phase was found in the XRD spectra. However, Co was found using XEDS in area 3 in Figure 6.8. It is not possible to say if it is pure Co or if Co is dissolved in an other phase, since the XEDS spectra also contained other elements. The location, close to the WC, is not strange since the Co also comes from the milling bodies.

After HPHT sintering W_2CoB_2 was found in the XRD spectra. Figure 6.14 reveal a structure with bright contrast that contain both W and Co. The relative amounts of W and Co atoms (50 cat% W to 22 cat% Co in area 1 and 22 cat% W to 11 cat% Co in area 2) makes W_2CoB_2 a probable phase. The rest of the cations were Al, that is probably mostly from the surrounding Al-rich dark grey phase.

7.2 Cermet milled materials

The cermet milled materials show a wide diversity in composition and local structure. The microstructures are more complex than in the WC-Co milled materials.

7.2.1 Powder characterisation

Just as in the WC-Co milled materials, the specific surface area of the starting powder mixture increased with increased milling time. The area was larger than for the WC-Co milled case. This is probably due to the much longer milling time for the cermet milled materials. The use of cermet milling bodies enables a more fine grained starting powder mixture without introducing an increased amount of W.

7.2.2 Phase composition

For the cermet milled materials some other phases are created during the densification process, as seen in the results chapter. Here the Ti(C,O,N), AlCo, Co- and Al-rich grain boundary phases, Al_2O_3 and TiB_2 are discussed.

Ti(C,O,N) with different compositions

During the pre sintering there seems to be no change in the lattice parameter of the Ti(C,O,N), see Table 6.14. The Ti(C,O,N) powder had probably not started to react during the pre sintering. Though, there might be a small change in the shape of the milling body shoulder of the Ti(C,O,N) 200 peak, seen Figure 6.18. This might imply some reactions in the milling body debris, but not in the Ti(C,O,N) raw material.

When looking at the structure of the pre sintered materials in Figures 6.21 and 6.22 the first difference from the pre sintered WC-Co milled materials is the shape of the grains. The raw, edgy grains seem to not have started sintering during the pre sintering and kept their sharp edges. However, we know from XRD that some reactions have occurred, since AlCo is present after pre sintering.

The identification of the phases in the pre sintered material 7 in Figure 6.21 is less straight forward than for the WC-Co milled materials. The more W an area contain, the brighter is the contrast in the SEM image. W and Ti are detected in all areas marked. Areas 1, 2, 3, 4 and 6 only contain W and Ti cations. These areas might be cermet milling body debris. The cermet milling bodies contain 17.8 wt% W and 49.0 wt% Ti, see Table 5.3. This gives a Ti:W atomic ratio of 10.6, which should be the average in the mill debris. The cermet have very different amounts of W in the structure, however, and thus the Ti:W ratio of the debris might vary. For the areas marked in the figure this ratio varies from 2.8 up to 11.5, most of them containing more W than the milling body average.

In the image of the pre sintered material 12 in Figure 6.22 the area marked 4 contain the highest amount of Ti of the areas investigated. It might contain Ti(C,O,N) from the raw material.

The HPHT sintered materials seem to show the same diversity in structures as the pre sintered ones. Figure 6.24 is an example of this. (a) and (b) are fairly close to each other. However, the structures are very different. In (a) the grains are well defined, homogeneous and have sharp edges. In (b) the grain boundaries are harder to define, some of the grains seem to have a gradient in the contrast and some seem to have a core- rim-structure. The grains are surrounded by a Co-rich phase. Area 1 and 4 in figure (a) have a similar composition and contain the smallest amount of W. These areas contain W, Al, Ti and Co and do not mach any of the phases found with XRD. These grains have formed during HPHT sintering and remain unidentified. Other techniques are needed to further characterise them. Area 2 and 3 contain no Al, but more W and 2 also contain Co. 2 is fairly close to a bright grain boundary phase, that might give the Co signal. Thus, the areas might be (Ti,W)(C,O,N). This phase might come from the cermet milling bodies (Ti,W)(C,N) grains, or from the initial Ti(C,O,N) powder that may have reacted with W.

Another example of an area containing both W, Al, Ti and Co is area 5 in Figure 6.28. This

area is close to the very W-rich area 4 with bright contrast, that is probably a (Ti,W)(C,O,N) grain. Area 3 also contain many different cations and is therefore not identified either.

In Figure 6.25 three different contrasts are marked. The main difference between those is the amount of W. Area 1 that is the darkest get 7.7 cat% when analysed with XEDS. This W might be in the actual dark grain, but it might possibly come from the very bright W-rich area around it. Area 3 contain some Al and the same thing applies here, the Al might come from another structure or might be in the actual phase investigated. The structure looks like a typical cermet core-rim structure. The (Ti,W)(C,N) grains from the cermet milling bodies may be retained in the HPHT sintered structure. A similar feature can be seen further down in the same micrograph.

The HPHT sintered material does not have the peak and the shoulder in the spectrum of the 200 Ti(C,O,N) peak, Figure 6.18. This means that it has probably reacted and formed a wide diversity of compositions, making the peak broaden. The peaks shift in the opposite direction in the WC-Co milled materials, as can be seen in Table 6.14. The peaks shift to higher 2θ in the cermet milled materials, giving smaller lattice parameters instead of larger as in the WC-Co milled materials. In the WC-Co milled materials the main reaction taking place is thought to be O from the Ti(C,O,N) reacting with Al and forming Al_2O_3. This probably happens in the cermet milled materials as well. However, W is detected in basically all Ti-rich phases in the cermet milled materials when XEDS is performed. The Ti(C,O,N) peak get closer to the (Ti,W)(C,N) peak of the cermet milling bodies. Thus, the W might affect the lattice parameter in the other direction and in larger extent than the loss of O.

An important difference from the WC-Co milled materials is the source of the Ti-rich phase. In the WC-Co case the Ti(C,O,N) only comes from the initial Ti(C,O,N) powder. The main Ti-rich phase in the WC-Co milled materials do not contain W. However, in the cermet milled case, there is a very similar phase in the milling bodies. The (Ti,W)(C,N) grains in the cermet have a core/rim structure as described in section 5.1, making the (Ti,W)(C,N) milling debris containing different amounts of W and Ti. In the end this might contribute to a broad variety in the stoichiometry in the (Ti,W)(C,O,N) phase of the sintered materials.

AlCo

Before sintering Co-containing phases are not found in the XRD spectra of the cermet milled materials, see Figure 6.15. The XRD for the pre sintered cermet milled materials contain some new peaks and have some of the old ones left as seen in Figure 6.16. The peaks identified as Al are gone, and instead AlCo peaks have appeared. In those pre sintered materials the Al, that is the first element to become liquid (at approximately $660\,^{\circ}C$ [17]) reacts with the Co. Co is much more abundant than in the WC milled materials. The amount of W, however, was the same after WC-Co and cermet milling, so there might have been a possibility to form the same Al-W phases as in the WC-Co milled materials. The W is however in different types of structures in the milling bodies, which might give the W different accessibility.

XEDS was performed in the different areas of the pre sintered material 7 marked in Figure 6.21. Al and Co is only detected in area 5, 7 and 8. Though, these areas do not look very different from the others marked in the micrograph. Figure 6.22 also contain a diversity of compositions. In this figure there are a number of areas containing more Al than Co. This does

not correspond to any phase identified in the XRD spectrum. However, Al is found everywhere, except for area 1, in this micrograph. The Al might be a thin grain boundary phase, on the surface of most grains but in very small amounts and therefore not detected in the XRD.

The HPHT sintered materials also have new phases, as seen in Figure 6.17. Here we have two unidentified phases with only one peak each, marked as Unid. 1 and Unid. 2 in the figure. Material 9 is the only material with a peak for the Unid. 2 phase. A guess based on the elements present in the materials is that Unid. 1 is CoB_2 and Unid. 2 is AlCo. Those are the phases that are marked with dark green and blue markers in the spectra. The only peaks present seem to correspond to the peaks with highest intensity in the data base spectra. AlCo was present after pre sintering, but this peak has shifted slightly after the HPHT sintering.

Grain boundaries

As seen in the results part, two different types of thin grain boundary films were found, containing Co and Al respectively. An example of the Co-rich phase can be seen in Figure 6.24(b) around the round, Ti-rich grains. The small size of the areas makes it impossible to tell the exact composition of the phase with the techniques used.

Figure 6.26 also contain the grain boundary phase. Area 1 is the Co-rich binder phase, but in this case it also contain some Mo. Mo is not part of the constituents of the raw materials added. It might come from the Mo-film used in the HPHT sintering process. This should be removed during the polishing of the specimen described in section 4.3. Worth noting is that the Mo is only found in the Co-rich binder phase. It was not possible to find Mo in all specimen. Probably this is due to the Mo only being close to the surfaces of the materials, and hence only present where the specimens were not polished long enough. What could be done is to polish the side of the square specimen and map these. Then a cross section of the height can be investigated in order to see if there is only Mo at the surface.

An example of the Al-rich grain boundary phase can be seen in Figure 6.28. The melting temperature of Al is $660\,°C$ [17] and thus the Al would have been liquid during the HPHT sintering. The shape of the dark grey phase makes it also look like it has formed during sintering. The Al-rich phase seem to have solidified between the two Ti-rich grains, filling out the triangular space between them.

Al_2O_3

After HPHT sintering Al_2O_3 is found in the XRD spectrum of material 10. Two examples of Al-rich features in this material is shown in Figure 6.27. Al is found both in the small, round features in the Ti- and W-rich areas and close to the cBN grain. Material 10 is special in that it contains the highest amount of Al according to chemical analysis, 4.9 wt%, see Table 6.10. Material 11, that is also a high Al-content material only contains 3.9 wt% Al, for comparison. The WC-Co milled material generally contained more Al than the cermet milled ones according to chemical analysis, see Table 6.1. Al_2O_3 was found in the XRD spectra for all WC-Co milled materials after HPHT sintering.

However, Al-rich, small features are found in all the cermet milled materials using XEDS, and might be Al_2O_3, in too small amounts to be found with XRD. One example is the dark

grey feature between area 1 and 2 in Figure 6.24(a). Another possible phase is AlN that was found in the WC-Co milled materials.

TiB$_2$

In the XRD spectra, material 10 is the only one where there are distinguishable TiB$_2$ peaks. In Figure 6.27 the large area with grey contrast in the middle contain Ti. The XEDS spectra do also contain a B peak, that is not common for all Ti-rich areas. This suggests that this is a large TiB$_2$ grain. The grain shape looks like the phase has formed during sintering. The phase seem to fill out the space between other grains. The B comes from the cBN so if there is no cBN grain next to the TiB$_2$, B must have been transported through other phases.

8

Conclusions

The WC-Co milled and the cermet milled materials behave differently during pre sintering at 900 °C. The WC-Co milled materials start to sinter. The HPHT sintered WC-Co milled materials have W-rich films between the Ti(C,O,N) grains. The HPHT sintered cermet milled materials have either Co-rich or Al-rich films between the (Ti,W)(C,O,N) grains. The phases created are dependent on the raw material composition. The amounts of Al, W and Co affect both the pre sintered and the HPHT sintered phase compositions. There are very many local equilibrium rather than a global equilibria when the sintering is stopped. Especially the cermet milled materials show a wide diversity in local structure and composition.

9

Further work

There are several things that would be interesting to investigate further. First, it would be interesting to continue the work to understand the microstructures on a finer scale. The microstructures contain a lot of interesting, very small, features that were not possible to get much information about in the SEM due to the limited resolution. Therefore other techniques are needed, like TEM/XEDS/EELS. The exact composition would also be interesting to investigate further, to get more understanding of what reactions are taking place and where the different elements come from and end up in the structure. The amount of the lighter elements C, O and N in different phases would be interesting to know more about.

Since the reactions seem to have stopped when the sintering stopped it would also be interesting to investigate longer sintering times. In this project the materials were HPHT sintered for 45 minutes, but interesting would be to see what has happened after, lets say, one hour or one and a half.

Finally, this project has not included any investigations of the performance of the materials as cutting tools. Therefore, a proper testing of the materials would be of importance to investigate their mechanical properties and thereby their suitability as tool materials. The connection between the microstructure and the performance of the tools could then be mapped.

Bibliography

[1] Koepfer, C. (2005) Tooling up for hard turning. *Production Machining.* http://www.productionmachining.com/articles/tooling-up-for-hard-turning (2013-04-20).

[2] Angseryd, A. (2011) *Microstructure of a cubic boron nitride tool material and its degradation during hard turning operations.* Göteborg: Chalmers University of Technology. (Doctoral Thesis at the Department of Applied Physics).

[3] Benko, E. et al. (1999) cBN-TiN, cBN-TiC composites: chemical equilibria, microstructure and hardness mechanical investigations. *Diamond and Related Materials,* vol. 8, no 10, pp. 1838-1846.

[4] Rong, X.-Z. et al. (2002) High-pressure sintering of cBN-TiN-Al composite for cutting tool application. *Diamond and Related Materials,* vol. 11, no 2, pp. 280-286.

[5] Wentorf , R. H. Jr. (1957) Cubic Form of Boron Nitride. *Journal of Chemical Physics,* vol. 26, pp 956.

[6] Fukunaga, O. (2000) The equilibrium phase boundary between hexagonal and cubic boron nitride. *Diamond and Related Materials,* vol. 9, no 1, pp. 7-12.

[7] Wentrof, R. H., DeVries, R. C. and Bundy, F. P. (1980) Sintered Superhard Materials. *Science,* vol. 208, no 4446 pp 873 - 880.

[8] German, R. M., Suri, P. and Park, S. J. (2009) Review: liquid phase sintering. *Journal of Material Science,* vol. 44, no 1, pp. 1-39.

[9] Kingery, W. D., Bowen, H. K. and Uhlmann, D. R. (1976) *Introduction to ceramics.* 2nd Edition. New York: John Wiley & Sons.

[10] Kang, S.-J. L. (2005) *Sintering: densification, grain growth, and microstructure.* [E-book]. Oxford: Elsevier Ltd Butterworth Heinemann.

[11] Benko, E. et al. (2003) Electron microscopy investigations of the cBN-Ti compound composites. *Materials Chemistry and Physics,* vol. 81, no 2-3, pp. 336-340.

[12] Brouwer, P. (2010) *Theory of XRD: Getting acquainted with the principles.* Almelo: PAN-alytical BV.

[13] Waseda, Y., Matsubara, E. and Shinoda, K. (2011) *X-Ray Diffraction Crystallography* [E-book]. Heidelberg: Springer.

[14] Goldstein, J. et al. (2003) *Scanning electron microscopy and X-ray microanalysis.* [E-book]. New York: Springer.

[15] Lindahl, P. (1995) *Microstructure of Cermets.* Göteborg: Chalmers University of Technology. (Doctoral thesis at the Department of Physics).

[16] International Centre for Diffraction Data, *Powder diffraction file*, using DIFFRAC.SUITE EVA software from Bruker.

[17] Clark, W. D. (1940) The Aluminium-Tungsten Equilibrium Diagram. *Journal: Institute of Metals*, vol. 66, pp. 271-286.